LAWRENCE
LIVERMORE
NATIONAL
LABORATORY

LLNL-JRNL-477551

The experimental liquid-vapor phase diagram of bulk nuclear matter

L. G. Moretto, J. B. Elliott, L. Phair, P. T. Lake

March 31, 2011

Journal of Physics G: Nuclear and Particle Physics

Disclaimer

The experimental liquid-vapor phase diagram of bulk nuclear matter

L. G. Moretto[1], J. B. Elliott[2], L. Phair[1] and P. T. Lake[1]

[1]Lawrence Berkeley National Laboratory, One Cyclotron Road, Berkeley, CA 94720
[2]Lawrence Livermore National Laboratory, 7000 East Avenue, Livermore, CA 94550

E-mail: elliott38@llnl.gov (LLNL-JRNL-477551)

Abstract.

The modern investigation of clusters, for which $1 \ll N \ll \infty$ requires a generalization of the thermodynamics developed for infinite systems. For instance, in finite systems, phase transitions and phase coexistence become ill defined with ambiguous signals.

The existence of phase transitions in nuclear systems, in particular of the liquid-vapor kind, has been widely discussed and even experimentally claimed. A consistent and unambiguous approach to this problem requires a connection between finite systems and the corresponding infinite systems. Historically, this has been achieved at temperature $T = 0$ by the introduction of the liquid drop model and the extraction of the volume term, which is a fundamental quantity of nuclear matter.

The present work extends this approach to $T > 0$, by determining the liquid-vapor coexistence line and its termination at at critical point. Since there is no known experimental situation where a nuclear liquid and vapor are in coexistence, we establish a relationship between evaporation rates and saturated vapor concentration and characterize the saturated vapor with Fisher's droplet model. We validate this approach by analyzing cluster concentrations in the Ising and Lennard-Jones models and extracting the corresponding first order coexistence line and critical temperature. Since the vapor of clusters coexists with a finite liquid drop, we devise a finite size correction leading to a modified Fisher equation.

The application of the above techniques to nuclear systems requires dealing also with the Coulomb force. Nuclear cluster evaporation rates can be corrected for Coulomb effects and can be used to evaluate the cluster concentrations in the "virtual" equilibrium vapor. These cluster concentrations, determined over a wide temperature range, can be analyzed by means of a modified Fisher formula. This leads to the extraction of the entire liquid-vapor coexistence line terminating at the critical point. A large body of experimental data has been analyzed in this manner and the liquid-vapor phase diagram of nuclear matter has been extracted.

1. Prolegomenon

This article is not a review of nuclear multifragmentation and of related dynamical or statistical models. A variety of reviews on this subject is available for a thorough description and analysis of the field [1, 2, 3, 4, 5, 6, 7, 8, 9, 10]. Neither is it a review of theories of phase transitions in nuclei and small systems. Rather, it is a coherent, systematic approach towards the extraction of the liquid-vapor phase coexistence diagram for infinite, uncharged, symmetric nuclear matter from a variety of nuclear reactions. It is also an illustration of the hurdles one encounters in such an effort, such as finite size, Coulomb effects and lack of existence of stationary phases in equilibrium coexistence in the experimental environment.

2. Introduction

Phase transitions have a way of catching the attention of our collective scientific unconscious. The dramatic changes in structure, density and other parameters at times overwhelm our better judgement. We know, but forget, that (at least for first order transitions) these transitions can be described (and predicted) on the basis of the thermodynamic characterization of each individual infinite phase simply with the requirement of equal thermodynamic potentials (e.g. temperature, chemical potentials, etc.). No phase-phase interaction is needed.

It is a case of myth hiding triviality.

The advent of mesoscopic physics made the waters murkier by introducing the additional complication of finiteness. So it appeared that finite size effects multiplied the general thermodynamics of infinite systems into an infinity of thermodynamics, one for each finite system.

In nuclear physics this complication was partially avoided. On one hand, we dealt from the beginning with finite nuclei. On the other, we understood the danger of long range forces, such as the Coulomb force. Indeed, it was soon learned how to move elegantly from finite to infinite systems through the liquid drop model expansion [11, 12, 13].

In this way, to do justice to our forefathers, some properties of zero temperature, symmetric, uncharged nuclear matter were quickly determined from the volume term of the liquid drop expansion. The existence of a dilute gas-like phase at temperatures above zero became soon obvious as "hot nuclei" started evaporating neutrons under the hands of experimentalists [14, 15]. Thus, given the apparent existence of two phases, it was natural to inquire about their possible equilibrium coexistence.

Phase diagrams for ordinary physical/chemical systems are simple and fundamental road maps to guide one through the sometimes complicated coexistence of several "phases" in heterogeneous systems.

Gibbs' description of equilibria in such systems leads naturally to phase diagrams. The number of possible coexisting phases and the latitude of their coexistence is distilled

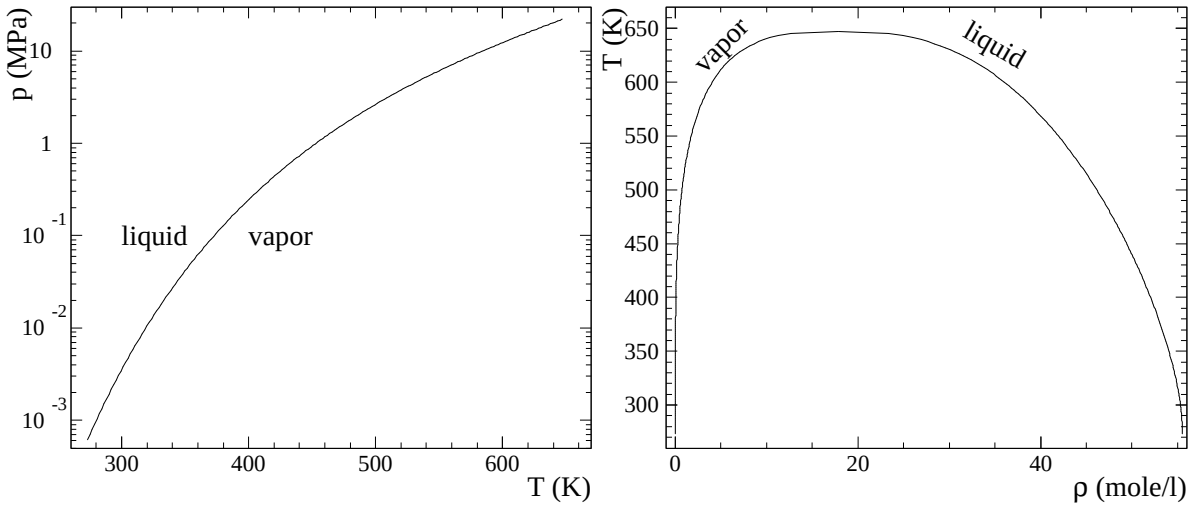

Figure 1. The liquid-vapor portion of the phase diagram of water (H_2O). The data was obtained from the NIST data base [16].

in the Gibbs "variance" equation

$$\nu = \eta - \phi + 2 \tag{1}$$

where ν, the variance, is the number of thermodynamic variables that must be specified in order to characterize the system. The number of independent components is η and the number of coexisting phases is ϕ.

For water ($\eta = 1$), let us consider only the liquid-vapor (l-v) transition:

$$H_2O_l \rightarrow H_2O_v \tag{2}$$

forgetting for the moment that the system admits several solid phases. Figure (1) shows how the pressure, temperature plane (p, T) is divided by the coexistence line. To its right is the region of a single phase (vapor), where the variance is $\nu = 2$ because we must specify two coordinates (p and T) in order to characterize the state of the system. Similarly, to the left of the coexistence line is the region of the liquid, and $\nu = 2$ for the same reasons. However, along the coexistence line both phases are present and $\nu = 1$. Thus a single variable, either T or p, completely fixes the state of the system. An equivalent and perhaps more familiar temperature–density (T, ρ) diagram is also shown in Fig. 1.

There is no single phase transition temperature. Boiling, a particular way that the system has to achieve coexistence, occurs at a temperature completely dependent on the applied pressure. Similar considerations can be made about the solid-liquid coexistence and the "melting" point, which also completely depends on the pressure.

After this parenthesis, we return to nuclear matter, and its definition. It has been long known that nuclei can be considered as charged droplets of a Van der Waals like fluid. Their binding energy E_A, or mass, can be written in terms of a volume term, a

surface term, a symmetry term and a Coulomb term as follows [11]

$$E_A = -a_V A + a_s A^{2/3} + a_{\rm sym}\frac{(N-Z)^2}{A} + a_{\rm C}\frac{Z^2}{A^{2/3}} + \ldots \tag{3}$$

where: a_V is the volume or bulk energy coefficient; A is the number of nucleons; a_s is the surface energy coefficient; $a_{\rm sym}$ is the symmetry energy coefficient; N is the number of neutrons in the nucleus; Z is the number of protons in the nucleus (and $A = N+Z$); and $a_{\rm C}$ is the Coulomb energy coefficient. For alternative formulae see references [17, 13].

Equation (3) can be used in two ways: on one hand, it can predict the binding energies of specific nuclei with an accuracy of about 1% ($\lesssim$ 10 MeV), and with shell corrections, easily obtainable from the shell model, binding energies accurate to within 1 MeV can be obtained [18, 19, 20]. On the other hand, one can discard all the terms other than the first and obtain the binding energy of the infinite, uncharged and N, Z symmetric system which we call bulk nuclear matter, a condensed fluid which, in many ways should resemble a Van der Waals liquid [21].

This information, together with the equilibrium density obtained from nuclear radii (also directly inferable from the Coulomb coefficient [12]) gives us a satisfactory "thermodynamical" characterization at zero temperature.

The Van der Waals features of this nuclear fluid immediately pose the question about its properties at higher temperatures. Is there a vapor-like phase? Can it coexist with the condensed liquid-like phase and over what temperature range? Is there a critical temperature at which the distinction between the two phases disappears [22]? In other words, can one obtain a pressure-density-temperature (p,ρ,T) phase diagram analogous to those shown in Fig. 1? This is our quest.

Let us consider the possibility of a vapor phase. It has long been known that an excited nucleus could emit neutrons with a thermal kinetic energy spectrum of the form

$$P\left(E_k\right) = \frac{16\pi}{h^3} m_n \sigma_n e^{-\frac{B_n}{T}} E_k e^{-\frac{E_k}{T}} \tag{4}$$

where E_k is the kinetic energy of the evaporated neutron; h is Planck's constant; m_n is the neutron mass; σ_n is the neutron capture inverse cross section; B_n is neutron binding energy; and T is the temperature [14, 15]. This expression is a re-writing of Weisskopf's formula which is, incidentally, identical to that for the thermionic emission of electrons from a hot filament and, apart from spin degeneracies, to that of the evaporation of molecules from the surface of a liquid.

The naming of this expression the "Weisskopf evaporation formula" indicates that the analogy with the liquid-vapor phase transition was already in the mind of the discoverer (and of his referees, if he had any). In fact, the absolute evaporation rate is equal, at equilibrium, to the condensation rate, which depends on the saturated vapor concentration. Therefore (barring Coulomb effects) "evaporation" implies the existence of a vapor phase, whether this phase is actually present or not. This is a key point, essential to achieving our goal. It is also a restatement of the "trivial" nature of first order phase transitions.

From eq. (4) which gives the rate of emission per unit surface, it is possible to obtain the pressure of the neutron vapor in equilibrium with a nucleus

$$p = \left(\frac{2\pi m_n T}{h^2}\right)^{3/2} 2Te^{-B_n/T}. \tag{5}$$

But what about the observed emission of protons or of heavier clusters? Do they belong to the vapor phase as well? This problem will be dealt with later on.

3. Thermodynamic frugality

If one is interested in calculating the pressure of the vapor in equilibrium with bulk nuclear matter, one can use the Claperyon equation

$$\left.\frac{dp}{dT}\right|_{\text{coex}} = \frac{\Delta H_e^m}{T\Delta V^m} \tag{6}$$

where ΔH_e^m is the molar enthalpy of evaporation and the change in molar volume $\Delta V^m \simeq V_v^m$ is taken to be the molar volume of the vapor at the ideal vapor approximation. One then obtains

$$\left.\frac{d\ln p}{dT}\right|_{\text{coex}} = -\frac{\Delta H_e^m}{T^2} \tag{7}$$

and taking the enthalpy of evaporation (work function) to be $\Delta H_e^m = -a_V + T$ one finally gets

$$p \simeq p' e^{-a_V/T} \tag{8}$$

where a_V is the volume term in the liquid drop model and p' is a slowly varying function of T. This should be an excellent guess, rather accurate at relatively low temperatures, where the vapor may be considered ideal and dominated by monomers.

All this is, in fact, rather trivial, requiring only knowledge of the "work function" a_V (which we get from the liquid drop) and of thermodynamics.

This much was implicitly known and could have been made explicit before 1940. Compare now equation (8) with the scaling expression used by Guggenheim [23] to fit the data in the left plot in Fig. 2 for a variety of Van der Waals systems

$$p = p_c \exp\left[-\frac{\Delta H_e^m}{T}\left(1 - \frac{T}{T_c}\right)\right] \tag{9}$$

where p_c and T_c are the critical pressure and temperature respectively. Equations (8) and (9) are obviously equivalent.

So, it appears that in order to obtain the full phase diagram of nuclear matter we must obtain the critical parameters from experiments. In order to obtain such parameters we should use the properties of the gas phase (vapor) in equilibrium with nuclear matter at $T > 0$. Unfortunately, we do not have access to such a system. However, we have the possibility of studying particles and clusters "evaporated" from hot finite nuclei. From these observations we may hope to extract the properties of the saturated vapor.

Three problems (at least) are to be overcome:

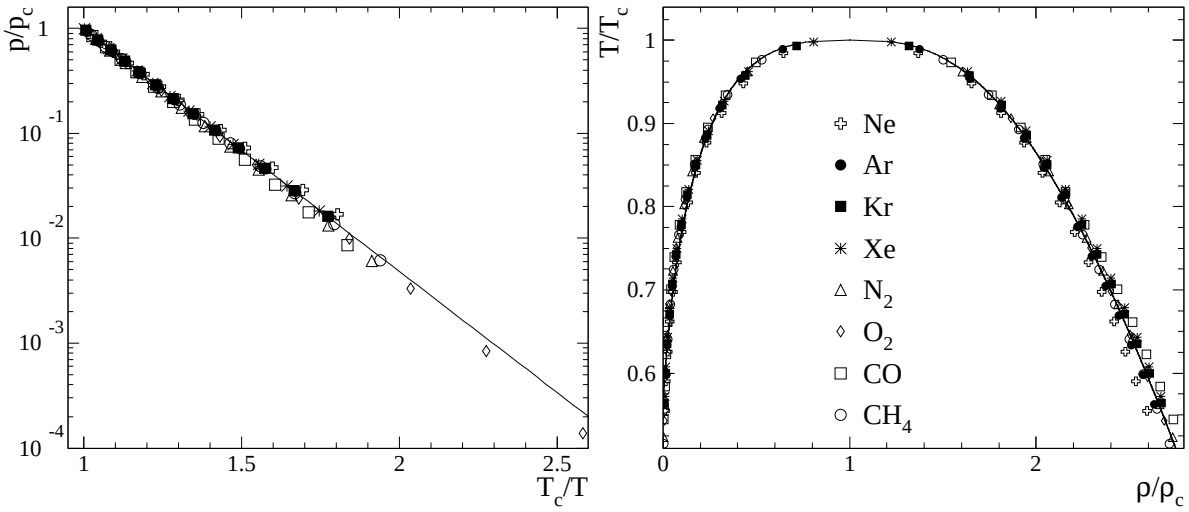

Figure 2. The reduced pressure as a function of the inverse of the reduced temperature (left) and the reduced density as a function of reduced temperature (right), à la Guggenhiem [23, 24]. Data for eight different fluids fall on the same curve. The data for the fluids was obtained from the NIST data base [16]. The pressure-temperature curve (left) is from reference [24] and the temperature-density curve (right) is from reference [23].

(i) no vapor is ever found in equilibrium with a hot nucleus, but (at least under most experimental conditions) emission (evaporation) occurs in vacuum [25];

(ii) the finiteness of nuclei affects the rate of emission of fragments [26].

(iii) Coulomb effects the relative abundance of fragments through the heights of the Coulomb barrier [27];

We address and overcome all these problems below.

4. Characterization of the saturated vapor phase through cluster distributions

Where and how can we obtain information about the vapor phase? Heavy ion reactions at intermediate and high energy produce abundant fragments whose energy and mass/charge distributions show strong signals of thermalization [28]. In particular, individual fragment multiplicities over a broad range of excitation energies can be reproduced by a Poissonian distribution (reducibility) [4] which indicates that the probability of emitting n fragments can be "reduced" to the probability of emitting just one. In turn, this elementary probability scales with excitation energy as a Boltzmann factor (thermal scaling), giving rise to remarkably linear Arrhenius plots [29, 30, 4]. See Figure 3.

Thus the evidence points to *stochastic*, *independent*, *thermal* fragment emission, and the connection of such a kind of multifragmentation with compound nucleus emission seems natural. Multifragmentation in these cases may be just the continuation of

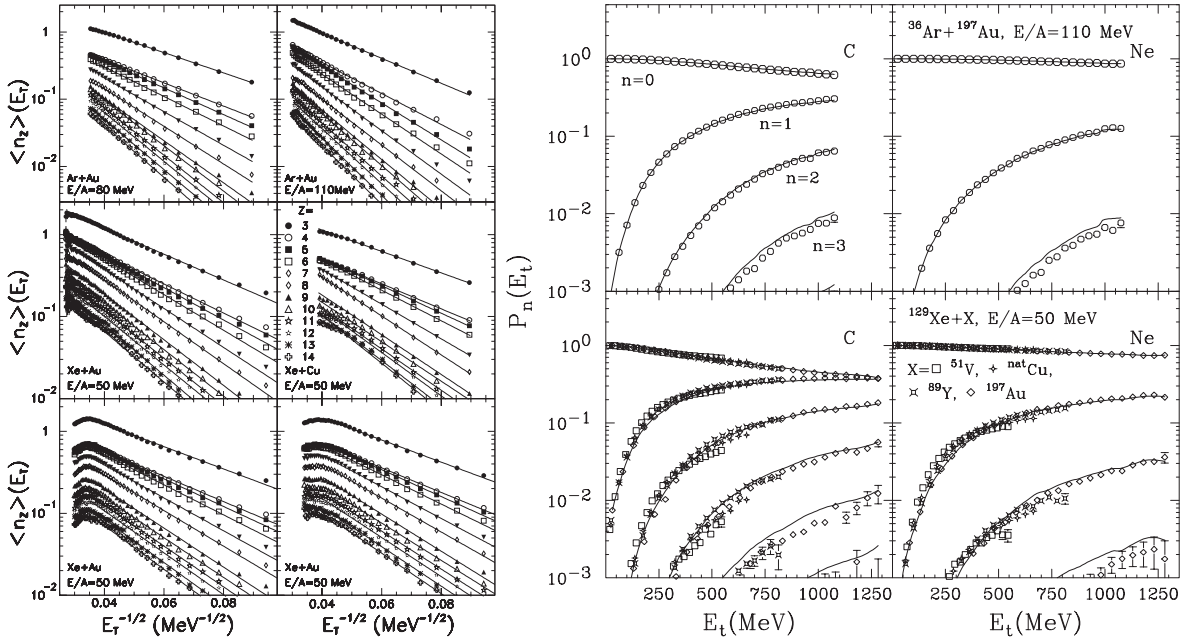

Figure 3. Left: The average yield as a function of the inverse of the square root of the transverse energy. The symbols show experimental data points while the solid lines show fits to the data using a Boltzmann form. Right: The excitation functions for carbon (left) and neon (right) emission. The symbols show experimental data points and the solid curves are Poisson fits. See reference [28] for further details.

compound nucleus emission at high energies, unfortunately with the added complication of uncertainties regarding the number and size of the sources, their excitation energies and their angular momenta.

In low energy compound nuclear reactions we have observed and characterized thermal emission (evaporation) of nucleons and clusters of nucleons [29, 30, 4]. The tendency of nucleons (monomers) to condense into clusters reflects the non-ideality of the vapor and contains information regarding the evolution of the vapor itself along the coexistence curve towards criticality.

We believe that, in nuclear physics, this is the royal avenue toward the extraction of the phase diagram, because cluster emission in nuclei or thermalized nuclear systems is readily and quantitatively observed.

The cluster size distribution in the (saturated) vapor can be adequately described in terms of the independent physical cluster models where the non-ideality of the vapor is taken to be exhausted in the formation of clusters that otherwise behave ideally [31, 32, 33, 34].

4.0.1. The physical cluster model Physical cluster theories of non-ideal fluids assume that the monomer-monomer interaction is exhausted in the formation of clusters, and that the resulting clusters behave ideally (i.e. they do no interact with each other) [31, 32]. Clusters of a given number of constituents A can be characterized by their

mass m_A, a chemical potential (per constituent) μ and a partition function $q_A(T,V)$ that depends on the temperature T and volume V of the fluid. Because of the ideality of the fluid of clusters, the pressure and density are readily determined. The pressure p is

$$p = \frac{T}{V}\sum_{A=1}^{\infty} q_A(T,V)z^A \tag{10}$$

and the density ρ is

$$\rho = \frac{1}{V}\sum_{A=1}^{\infty} Aq_A(T,V)z^A \tag{11}$$

where z is the fugacity $z = e^{\mu/T}$. The concentration of size A clusters is then

$$n_A(T,z) = \frac{q_A(T,V)z^A}{V}. \tag{12}$$

4.1. Fisher's theory

Fisher's contribution to physical cluster theory was to endow clusters with a surface energy and to provide an estimate for the entropic part of the free energy associated with the formation of a cluster [33, 34].

Fisher started by writing the energetic contribution to the free energy based on the liquid drop expansion

$$E_A = E_V + E_s \tag{13}$$

where E_V is the volume (or bulk) binding energy of the cluster which is taken to be

$$E_V = a'_V V \simeq a_V A. \tag{14}$$

Here V is the volume of the cluster; $a'_{\rm V}$ is the volume energy coefficient in terms of V; and a_V is the volume energy coefficient in terms of A. The term E_s is the loss of binding due to the surface s of the cluster. For clusters this is usually taken to be

$$E_s = a'_s s \simeq a_s A^{\frac{d-1}{d}} \tag{15}$$

where s is the surface area of the cluster; d is its dimensionality; a'_s is the surface energy coefficient in terms of s; and a_s is the surface energy coefficient in terms of $A^{\frac{d-1}{d}}$. The surface energy is written more generally as $E_s = a_s A^\sigma$ where σ is an exponent describing the relationship between surface and volume of the cluster. One intuitively expects that $\sigma \approx 2/3$ for three dimensional systems.

Fisher speculated that the entropic contribution to the free energy is dominated by the number of possible shape configurations g_A for a cluster of size A. For large clusters, over some small temperature range the most probable or mean surface of a cluster should be [33, 34]

$$\overline{s} \simeq a_0 A^\sigma \tag{16}$$

where a_0 is some constant of proportionality. The asymptotic number of shape configurations is written as

$$g_A \simeq g_0 A^{-\tau} e^{b_s A^\sigma} \tag{17}$$

where g_0 is a normalization constant, τ is an exponent that arises from studies of combinatorial problems [33, 34] and b_s is the surface entropy coefficient. The entropy of a cluster becomes:

$$S_A = \ln g_A = \ln g_0 - \tau \ln A + b_s A^\sigma. \tag{18}$$

Fisher's insight was to recognize that a cluster's energy and entropy share, to leading order, the same dependence on A, namely they are linear with A^σ, which makes the free energy of all cluster go to zero at the same "critical" temperature, as can be seen below.

Now, the partition function of a cluster is

$$q_A(T,V) = V \left(\frac{2\pi m_A T}{h^2}\right)^{\frac{d}{2}} \exp\left(-\frac{E_A - TS_A}{T}\right). \tag{19}$$

Combining equations (12), (13), (14), (15), (18) and (19) gives the number density of A as

$$n_A(T) = q_0 A^{-\tau} \exp\left(\frac{\Delta\mu A}{T}\right) \exp\left(-\frac{a_s \varepsilon A^\sigma}{T}\right) \tag{20}$$

where q_0 is a normalization constant, $\Delta\mu$ is a measure of the distance from coexistence in terms of the chemical potential and

$$\varepsilon = 1 - T\frac{b_s}{a_s} = \frac{T_c - T}{T_c} \tag{21}$$

with the critical temperature given by

$$T_c = \frac{a_s}{b_s}. \tag{22}$$

At saturation, $\Delta\mu = 0$, so there are no terms that depend on A to the first power.

4.1.1. Thermodynamic quantities from Fisher's model In order to obtain thermodynamic quantities such as pressure p and density ρ we combine the general equations for pressure and density for physical cluster theories with Fisher's estimate of the cluster partition function. Then, along the coexistence line, i.e. $\Delta\mu = 0$, we have

$$p_{\text{coex}} = T \sum_{A=1}^{\infty} q_0 A^{-\tau} \exp\left(-\frac{a_s \varepsilon A^\sigma}{T}\right) \tag{23}$$

and

$$\rho_{\text{coex}} = \sum_{A=1}^{\infty} q_0 A^{1-\tau} \exp\left(-\frac{a_s \varepsilon A^\sigma}{T}\right). \tag{24}$$

At the critical point we have

$$p_c = T_c \sum_{A=1}^{\infty} q_0 A^{-\tau} \tag{25}$$

and

$$\rho_c = \sum_{A=1}^{\infty} q_0 A^{1-\tau}. \tag{26}$$

Taking ratios from equations (23) to (26) we obtain the reduced pressure

$$\frac{p_{\rm coex}}{p_c} = \frac{T \sum_{A=1}^{\infty} A^{-\tau} \exp\left(-\frac{a_s \varepsilon A^{\sigma}}{T}\right)}{T_c \sum_{A=1}^{\infty} A^{-\tau}} \tag{27}$$

and the reduced density

$$\frac{\rho_{\rm coex}}{\rho_c} = \frac{\sum_{A=1}^{\infty} A^{1-\tau} \exp\left(-\frac{a_s \varepsilon A^{\sigma}}{T}\right)}{\sum_{A=1}^{\infty} A^{1-\tau}} \tag{28}$$

which have the advantage of being free of the constant q_0.

Thus we see how to infer the phase diagram from cluster distributions. We put this to the test below.

4.2. Application of the cluster approach to mathematical models

The models in the following sections are well understood and their phase diagrams known. We will try to derive the phase diagrams with the method illustrated above. As an aside, we note that thermodynamicians would not go through the trouble of constructing a phase diagram based on clusters as we do below. They would simply measure the pressure, density and temperature of their fluid. However, measurements of temperature, density and pressure for a nuclear fluid are problematic. On the other hand, the measurement of clusters in nuclear reactions has been easily achieved and has a long tradition. Thus our interest in using clusters to construct the phase diagram.

4.2.1. The Ising (lattice gas) model The Hamiltonian of the Ising model has two terms: the interaction between nearest neighbor spins $\mathcal{S}$ on a fixed lattice and the interaction between the spins and an external applied field H_{ext}:

$$H = -\sum_{i,j} \mathcal{J}_{i,j} \mathcal{S}_i \mathcal{S}_j - H_{ext} \sum_i \mathcal{S}_i \tag{29}$$

where the subscripts i and j label lattice sites and $\mathcal{J}_{i,j}$ is the strength of the spin-spin interaction which is equal to $\mathcal{J}$ if i and j are neighboring sites with aligned spins and equal to zero if not. For dimensions greater than or equal to two, in the absence of an external magnetic field, the system exhibits a first-order phase transition for temperatures up to the critical point at which it exhibits a continuous phase transition.

The zero-field Ising model is isomorphous with the lattice gas model at coexistence [35, 36]. The down spins are mapped to unoccupied sites in a lattice gas and the up spins are mapped to occupied sites. The phase transition in the Ising model is then analogous to a liquid-vapor phase transition.

The results shown here are taken from calculations performed via a code using standard Monte Carlo techniques [37]. After the system was thermalized, geometric clusters, i.e. nearest neighbor like spins, were identified and then the Coniglio-Klein

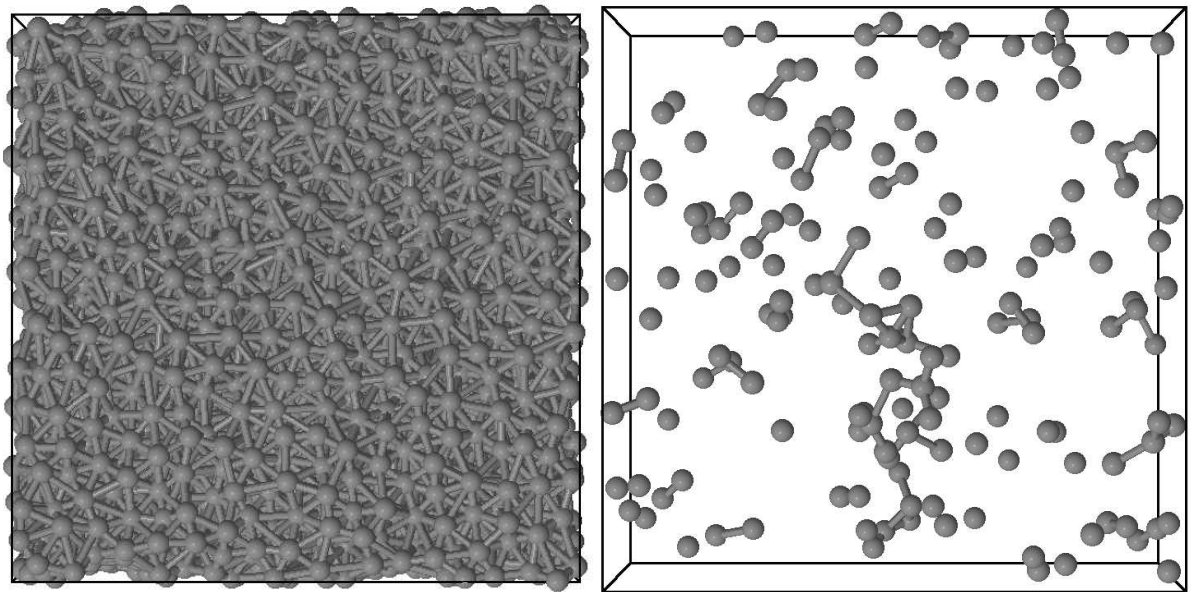

Figure 4. Left: The liquid phase. Right: The vapor phase. The gray spheres show the particles. Clusters are shown by particles connected with gray cylinders. Lines show the edges of the cubic container.

algorithm [38] was used to break the geometric clusters into physical clusters. All calculations were performed at zero external field ($H_{ext} = 0$). The lattice contained 50^3 spins, and periodic boundary conditions were adopted to minimize finite size effects. We used of the Swendsen-Wang algorithm and Coniglio-Klein clusters to insure that the clusters analyzed in this work are most closely related to the physical clusters observed in fluids [39, 40].

4.2.2. The Lennard-Jones (molecular dynamics) model In addition to the Ising model, the same phase transitions and cluster scaling were studied in a system of particles interacting though the Lennard-Jones pairwise potential. In this model, the potential energy of two particles separated by a distance of r_{ij} is

$$V_{LJ}(r_{ij}) = -4\epsilon \left[\left(\frac{r_{\mathrm{LJ}}}{r_{ij}} \right)^{-6} - \left(\frac{r_{\mathrm{LJ}}}{r_{ij}} \right)^{-12} \right]. \tag{30}$$

The system is characterized by two parameters ϵ and r_{LJ} which are measures of the characteristic energy and distance, respectively. This system exhibits a first-order phase transition at low temperatures, which terminates at a critical temperature with a continuous transition.

The Lennard-Jones model is not constrained to a lattice as is the Ising model. This makes the system more analogous to physical systems which we wish to study, be they atomic or nuclear systems.

An efficient means of studying coexistence in such a system is the Gibbs ensemble method [41]. The premise of such a calculation is that the two phases do not need to

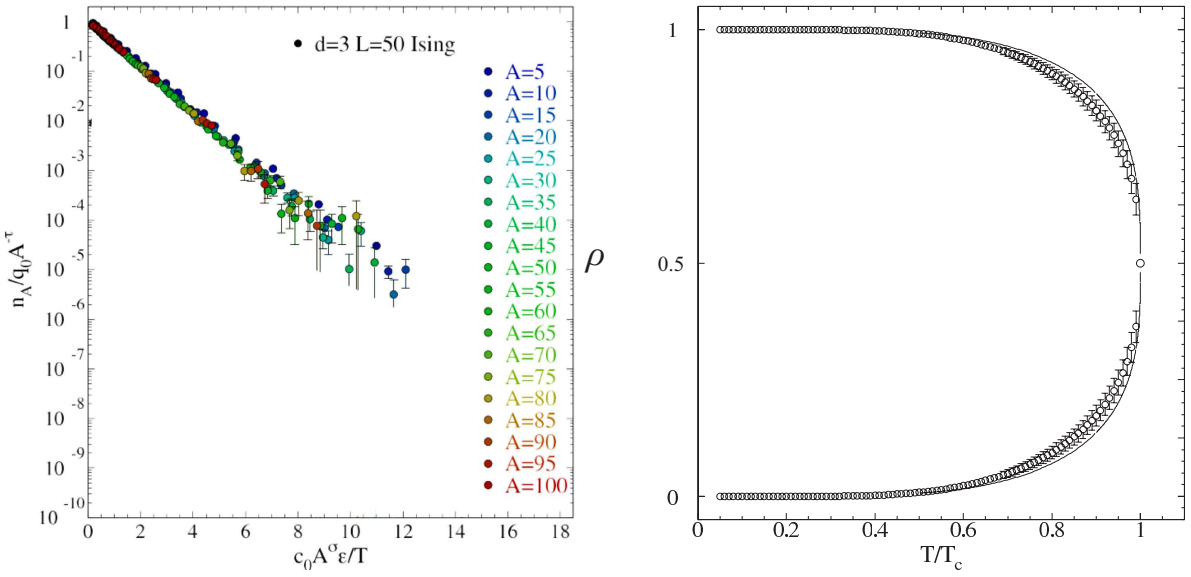

Figure 5. Left plot: the scaling of Eq. (32) for $d = 3$ Ising model on the simple cubic lattice of side $L = 50$ [43]. Here $c_0 = a_s$. Right plot: the density as a function of reduced temperature. The open circles show the density obtained from clusters via Fisher's theory and the solid line shows the actual density. See text for detailes

be in physical contact to study coexistence. Instead, two systems are made, one being of higher density and the other low. A Monte Carlo simulation is performed at a given temperature, allowing the two systems to exchange volume and particles, establishing equal pressures and chemical potentials in the two containers. No prior knowledge of the coexistence density, pressure, or chemical potential is needed.

For this study a system of 4,800 particles was considered. The containers of the two phases were cubic and approximately equal in volume, resulting in a length of about $20r_{LJ}$. Six temperatures were considered in the range of $0.76 \leq T/T_c \leq 0.95$. Figure 4 give a sample configuration of the system.

Clusters were defined using the Hill algorithm [42]. This approach is based not only on geometric constraints, but also considers the momentum space of the constituents. Two nearby particles i and j are bound together if

$$\frac{m}{4}(\overrightarrow{v_i} - \overrightarrow{v_j})^2 \leq -V_{LJ}(r_{ij}), \tag{31}$$

where m is the mass of a particle and $\overrightarrow{v_i}$ is the velocity of the $i^{\underline{\text{th}}}$ particle.

4.3. Cluster scaling from Fisher's theory

4.3.1. Scaling of the Ising cluster distributions We start by considering the observed cluster concentrations in terms of Fisher's theory given by Eq. (20). Working at coexistence ($\Delta\mu = 0$) and dividing both sides by the power law factor, we obtain:

$$\frac{n_A(T)}{q_0 A^{-\tau}} = \exp\left(-\frac{a_s \varepsilon A^{\sigma}}{T}\right). \tag{32}$$

-	theoretical values	$L = 50$ calculations [43]
T_c	4.51152 ± 0.00004 [44]	4.52 ± 0.01
σ	0.63946 ± 0.0008	0.723 ± 0.008
τ	2.209 ± 0.002	2.30 ± 0.08

Table 1. Fit results for the $d = 3$ Ising model with $L = 50$ on the simple cubic lattice. The values of σ and τ are determined via exponent scaling relations: $\beta = (\tau - 2)/\sigma$ and $\gamma = (3 - \tau)/\sigma$ [33, 34] with $\beta = 0.32653 \pm 0.00010$ and $\gamma = 1.2373 \pm 0.002$ [45]. The deviation observed in the fitted result for σ arises from the unaccounted curvature of the clusters [46].

-	theoretical values	Gibbs
T_c	1.3120 ± 0.0007 [48]	1.368 ± 0.002
σ	0.63946 ± 0.0008	0.744 ± 0.002
τ	2.209 ± 0.002	2.199 ± 0.005

Table 2. Fit results for the Lennard-Jones system. The deviation observed in the fitted result for σ arises due to the curvature of the clusters [46].

Thus, plotting the logarithm of the left hand side versus the argument of the exponential on the right should yield a straight line irrespective of the temperature T or cluster size A. Figure 5 shows this type of scaling and data collapse in the Ising model cluster yields [43] and Table 1 gives the parameters obtained in the fit. These results show that the cluster analysis successfully yields the parameters necessary to construct the coexistence curve up to the critical temperature.

In order to further test the results above, we examine the density of the vapor

$$\frac{\rho_{\mathrm{v,l}}}{\rho_c} = \frac{1 \pm |M|}{2} \tag{33}$$

which we determine using Eq. (28). Putting the values of σ, τ, a_s and T_c (listed in Table 1 and determined from fitting clusters on the $d = 3$ Ising lattice shown in Fig. 5 [43]) in Eq. (28), Eq. (33) gives the vapor branch of the density curve. Due to the symmetry of the Ising model, the points showing the liquid density ρ_{l} are reflections about $\rho_c = 1/2$. The results are shown as the open circles in the right plot of Fig. 5.

These results compare well with a parametrization for the density determined using a functional form of $M(T)$ taken from the literature [47] and shown as a solid line in the right plot of Fig. 5. The agreement between the density values calculated via Eq. (33) and the $\rho(M(T))$ parameterization for $0 < T < T_c$ suggest that the ideal gas assumptions in Fisher's theory allow for an accurate description of the system even up to densities as high as ρ_c.

4.3.2. Scaling of the Lennard-Jones cluster distributions Now we examine the cluster distributions observed in the simulations of the Lennard-Jones system described above.

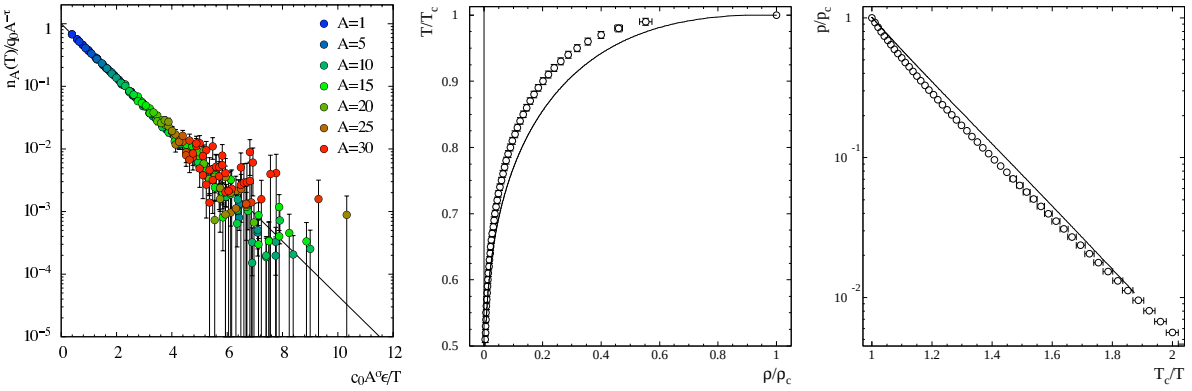

Figure 6. Left plot: the scaling of Eq. (32) for Lennard-Jones model Gibbs ensemble calculations. Here $c_0 = a_s$. Middle: the reduced density as a function of reduced temperature. Right: the reduced pressure as a function of the inverse of the reduced temperature. The open circles show estimates based on Fisher's droplet model. The solid line is from the NIST data [49].

As with the Ising model, the cluster distributions can be fit with Eq. (32) as shown in figure 6 and yields a value of T_c that agrees well with those in the literature as shown in Table 2.

As in the case with the Ising model, the value of σ is larger than that expected for its universality class. This consistent inconsistency stems from the fact that smaller clusters are being used for the fitting, whereas σ is a well defined quantity for appreciably larger clusters.

The reduced phase diagrams of the system are constructed by using equations (27) through (28) using the parameters listed in Table 2. These results are shown by the solid red squares in Fig. 6. Figure 6 also shows the reduced phase diagram determined by more traditional means [49]. The extracted phase diagrams are accurate at lower temperatures, but differ somewhat near the critical temperature.

5. Finite size effects: the complement method

Finite size effects are essential in the study of nuclei and other mesoscopic systems for opposite, but complementary reasons. In modern cluster physics, the problem of finite size arises when attempts are made to relate known properties of the infinite system to cluster properties brought to light by experiment [50]. For nuclear physics, the problem is the opposite: finite size effects dominate the physics at all excitations and the challenge lies in generalizing specific properties of a *drop* (nucleus) to the properties of uncharged, symmetric infinite nuclear matter. This goal has been achieved already for cold nuclei by the liquid drop model as discussed previously.

The finite size effects of having a liquid drop embedded in its saturated vapor are described by the Gibbs-Thomson equation [51]. Given a drop of size A_0, the pressure of the vapor, p, is greater than that of the coexistence pressure of a system with a planar

surface, $p_{\rm p}$, by the relation

$$\frac{p}{p_{\rm p}} = \exp\left(\frac{\sigma a_s A_0^{\sigma-1}\epsilon}{T}\right) = \exp\left(\frac{\Delta\mu_{\rm fs}}{T}\right). \tag{34}$$

Here, $\Delta\mu_{\rm fs}$ represents the shift in chemical potential as compared to the bulk coexistence chemical potential.

However, is a drop in "equilibrium" with its vapor truly stable? Consider a drop embedded in a bulk amount of vapor at the fixed equilibrium pressure given by Eq (34). Naturally, the drop size will fluctuate in size. If some material evaporates from the drop, the smaller drop will demand a larger external pressure. As a result, the drop will evaporate more and more until it disappears completely. Conversely, if some condensation occurs and the drop were to grow, it would require a lower pressure. As a result, the vapor continue to condense on the drop until it becomes a bulk sample of liquid. In this sense, a droplet is seen to be a state of unstable equilibrium.

A droplet may, however, exhibit stable equilibrium in a finite system which conserves the total number of particles. As fluctuations make the drop smaller in such a system, not only does the internal pressure of the drop increase, the surrounding vapor will also increase in pressure with the increase of particles into the vapor phase. Likewise, if the drop grows in size, the vapor pressure decreases with the transfer of particles into the liquid. Thus, the drop will evolve in size until a stable equilibrium is achieved.

One should notice that when we speak of finite size effects, we mean to draw attention to the finite size of the drop. It should not be confused with the concept of finite size corrections associated with the volume of the system studied in simulations [52]. These finite size corrections associated with the liquid drop have no relation to box size; surely, a compound nucleus will exhibit these finite size corrections, but there is no box in sight. The finite size effects due to the box size are present in our simulations but are minimized by choosing a large volume and periodic boundary conditions.

In this section, we present a general approach, which we call the complement method [26], to deal with finite size effects in phase transitions and illustrate it for liquid-vapor phase coexistence. The complement method consists of evaluating the free energy change occurring when a cluster of arbitrary size moves from one phase to another. For a finite liquid drop in equilibrium with its vapor, this is done by virtually transfering a cluster from the liquid drop to the vapor and evaluating the energy and entropy changes associated with *both* the cluster in the vapor *and* the residual liquid drop (or complement).

In this way, we generalize eq. (20) (at coexistence so that $\Delta\mu = 0$), valid for infinite liquid-vapor equilibrium, to the case of a vapor in equilibrium with a finite liquid drop. Fisher's expressions for $\Delta E_A(T)$ and $\Delta S_A(T)$ can be written for a drop of size A_0 in equilibrium with its vapor as

$$\Delta E_A(T) = a_s\left[A^\sigma + (A_0 - A)^\sigma - A_0^\sigma\right] \tag{35}$$

and

$$\Delta S_A(T) = \frac{a_s}{T_c}\left[A^\sigma + (A_0 - A)^\sigma - A_0^\sigma\right] - \tau \ln\left[\frac{A(A_0 - A)}{A_0}\right] \tag{36}$$

giving

$$n_A(T) = q_0 \left[\frac{A\,(A_0 - A)}{A_0}\right]^{-\tau} \exp\left\{-\frac{a_s \varepsilon}{T}\left[A^\sigma + (A_0 - A)^\sigma - A_0^\sigma\right]\right\} \tag{37}$$

which we call the generalized Fisher expression. This equation reduces to Eq. (20) *when A_0 tends to infinity*. Most importantly, it contains the parameters a_s and T_c of the *infinite* system. *Therefore, by fitting data from a finite system with Eq. (37), we automatically obtain the parameters for the infinite system.*

As an aside, we can rewrite Eq. (37) as

$$n_A(T) = n_A^\infty(T) \exp\left(\frac{A \Delta\mu_{\rm fs}}{T}\right) \tag{38}$$

with $n_A^\infty(T)$ given by Eq. (20) at coexistence. This shows that the finite size of the drop acts as an *effective* chemical potential which increases the vapor pressure [51] and is given by

$$\Delta\mu_{\rm fs} = -\frac{a_s \varepsilon\left[(A_0 - A)^\sigma - A_0^\sigma\right] - T\tau \ln\left(\frac{A_0 - A}{A_0}\right)}{A}. \tag{39}$$

Expanding this equation as a function of A/A_0, which will be small for large liquid drops, yields:

$$\Delta\mu_{\rm fs} \simeq a_s \epsilon \sigma A_0^{\sigma-1} - \frac{T\tau}{A_0} \tag{40}$$

which relates directly to the Gibbs-Thomson relation as seen in equation (34).

5.1. The complement and the lattice gas (Ising) model

In order to verify the complement method quantitatively, we apply it to the canonical lattice gas (Ising) model [35, 36] in two and three dimensions with a fixed number of occupied sites (up spins), i.e. a fixed mean occupation density $\langle\rho_{\rm fixed}\rangle$ in the lattice gas (equivalently, a fixed magnetization $M_{\rm fixed}$ Ising model) [53, 54]. For these calculations, at a temperature of $T = 0$ all the spins form a single cluster of size $A_{\rm d}^0$ (listed in Fig. 7) chose such that it is much smaller than the lattice in which it is embedded. At higher temperatures a drop (with size $A_0 < A_{\rm d}^0$) coexists with a vapor made up of $A_{\rm d}^0 - A_0$ constituents; A_0 depends on the temperature. Above the coexistence temperatures there is only a dilute vapor consisting of all $A_{\rm d}^0$ spins [54, 26].

We choose large lattices (i.e. large containers) with periodic boundary conditions in order to minimize finite lattice effects, irrelevant to our study. For $d = 2$ we use a square lattice of side $L = 80$ which leads to a shift in T_c of $\lesssim 0.5\%$ [55, 56]. For $d = 3$ we use a simple cubic lattice of side $L = 25$ which leads to a shift in T_c of $\lesssim 0.5\%$ [57, 58].

We also performed $\langle\rho_{\rm free}\rangle$ calculations (standard lattice gas calculations where the number of occupied sites is allowed to vary) for the same lattices as a benchmark in

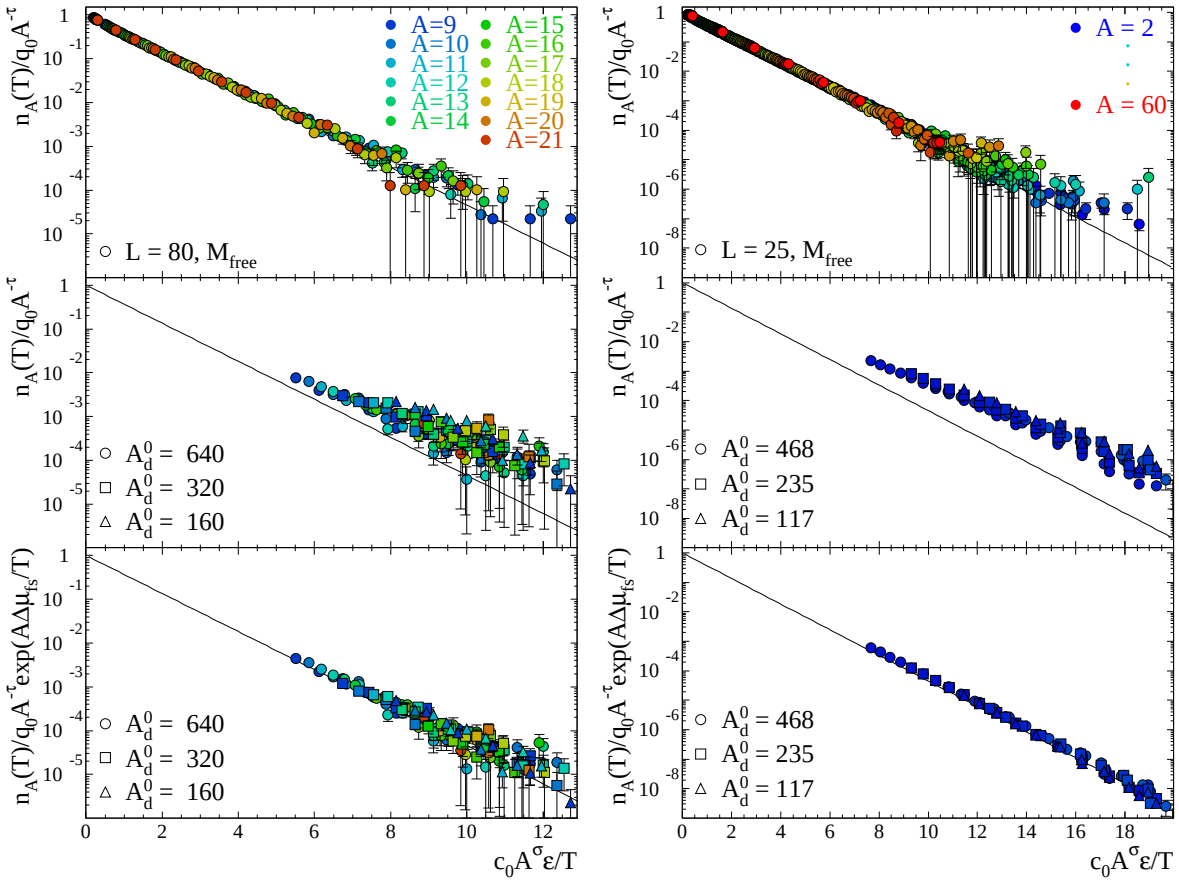

Figure 7. Left: The cluster concentrations of the $d = 2$, $L = 80$ periodic boundary condition square lattice for: $\langle\rho_{\rm free}\rangle$ calculations (top); $\langle\rho_{\rm fixed}\rangle$ calculations with no complement (middle); $\langle\rho_{\rm fixed}\rangle$ calculations with the complement (bottom). The color of the points reflect the size of the cluster. Right: results for the $d = 3$, $L = 25$ periodic boundary condition simple cubic lattice. The color of the points reflect the size of the cluster. For the $\langle\rho_{\rm fixed}\rangle$, $d = 3$ calculations, only small clusters were present. Only the top plots are the results of fits with free parameters. The middle and bottom plots are not fits and were made with no free parameters. Here $c_0 = a_s$.

order to differentiate effects of a finite lattice from those of a finite drop. The $\langle\rho_{\rm free}\rangle$ calculations emulate the vapor in coexistence with an infinite amount of liquid and thus have no explicit drop and are free of any complement effect. The cluster distributions of the $\langle\rho_{\rm free}\rangle$ calculations were fit with Eq. (20) with the free parameters T_c, a_s, σ, τ and the normalization set by the value of τ from the fit as

$$q_0 = \frac{1}{2\zeta(\tau - 1)} \tag{41}$$

to insure that the value of the critical density ($\rho_c = 1/2$) is recovered. Table 3 shows that the values of the T_c and τ returned by this procedure are within 1% of their established values. The top panels of figure 7 shows that, just as we saw in section 4.3.1, the cluster distributions collapse onto a single line by plotting $n_A(T)/q_0A^{-\tau}$ versus $a_sA^\sigma\varepsilon/T$.

However, plotting $n_A(T)/q_0A^{-\tau}$ versus $a_sA^\sigma\varepsilon/T$ (i.e. without the complement

-	Onsager [59]	this work	theoretical values	this work
-	$d = 2$	$d = 2$	$d = 3$	$d = 3$
-	$L \to \infty$	$L = 80$	$L \to \infty$	$L = 25$
T_c	$2.26915\ldots$	2.283 ± 0.004	4.51152 ± 0.00004	4.533 ± 0.002
σ	$8/15$	0.56 ± 0.01	0.63946 ± 0.0008	0.725 ± 0.003
τ	$31/15$	2.071 ± 0.002	2.209 ± 0.006	2.255 ± 0.001

Table 3. Fit results for $\langle \rho_{\rm free} \rangle$ calculations compared to accepted values found in the literature.

correction) using the parameters in Table 3 for the clusters in the $\langle \rho_{\rm fixed} \rangle$ calculations shows much less data collapse. This is show in the middle panels of figure 7.

The data collapse is recovered for the clusters in the $\langle \rho_{\rm fixed} \rangle$ calculations when plotting $n_A(T)/q_0 A^{-\tau} \exp\left[A\Delta\mu_{\rm fs}/T\right]$ versus $a_s A^{\sigma}\varepsilon/T$ (with the complement correction and again using the parameters in Table 3) as shown in the bottom panels of figure 7. The improvement in data collapse is clear from a visual inspection of figure 7, but can be quantified by constructing a χ^2. Doing this shows that the addition of the complement correction decreases, on average, the χ^2 by a factor of six [26].

Furthermore, when the complement correction is applied to clusters from the $\langle \rho_{\rm fixed} \rangle$ calculations, the data collapse to the same line as the data for the $\langle \rho_{\rm free} \rangle$ calculations. This demonstrates that information about the infinite system is accessible in finite systems when the effects of finite size are properly taken into account.

Finally, we emphasize that the middle and bottom panels of Fig. 7 do not show fits, i.e. those plots were made with no free parameters.

5.2. The complement and the Lennard-Jones model

To study the finite size effects discussed above for a system of a liquid drop in the Lennard-Jones system, molecular dynamics simulations were performed. The systems considered contained 600 particles in a spherical container. The radius of the container was $13.4 r_{LJ} \leq R \leq 24.3 r_{LJ}$. The temperature range of the simulations was $0.53 \leq T/T_c \leq 0.73$, the triple point of the system being at $T/T_c = 0.52$. The liquid drop sizes generated by these conditions were in the range of $110 \leq A_0 \leq 240$. A total of 30,000 configurations were sampled for 24 different energy–density combinations. A sample realization from the simulation is shown in figure 8.

Figure 9 shows the scaled cluster yields from the simulations using the fit parameters of the system studied with the Gibbs ensemble technique in section 4.2.2. The plot on the left shows the scaling without the complement correction, whereas the one on the right is with the complement correction. Droplets of such small size vividly demonstrate the importance of the complement correction.

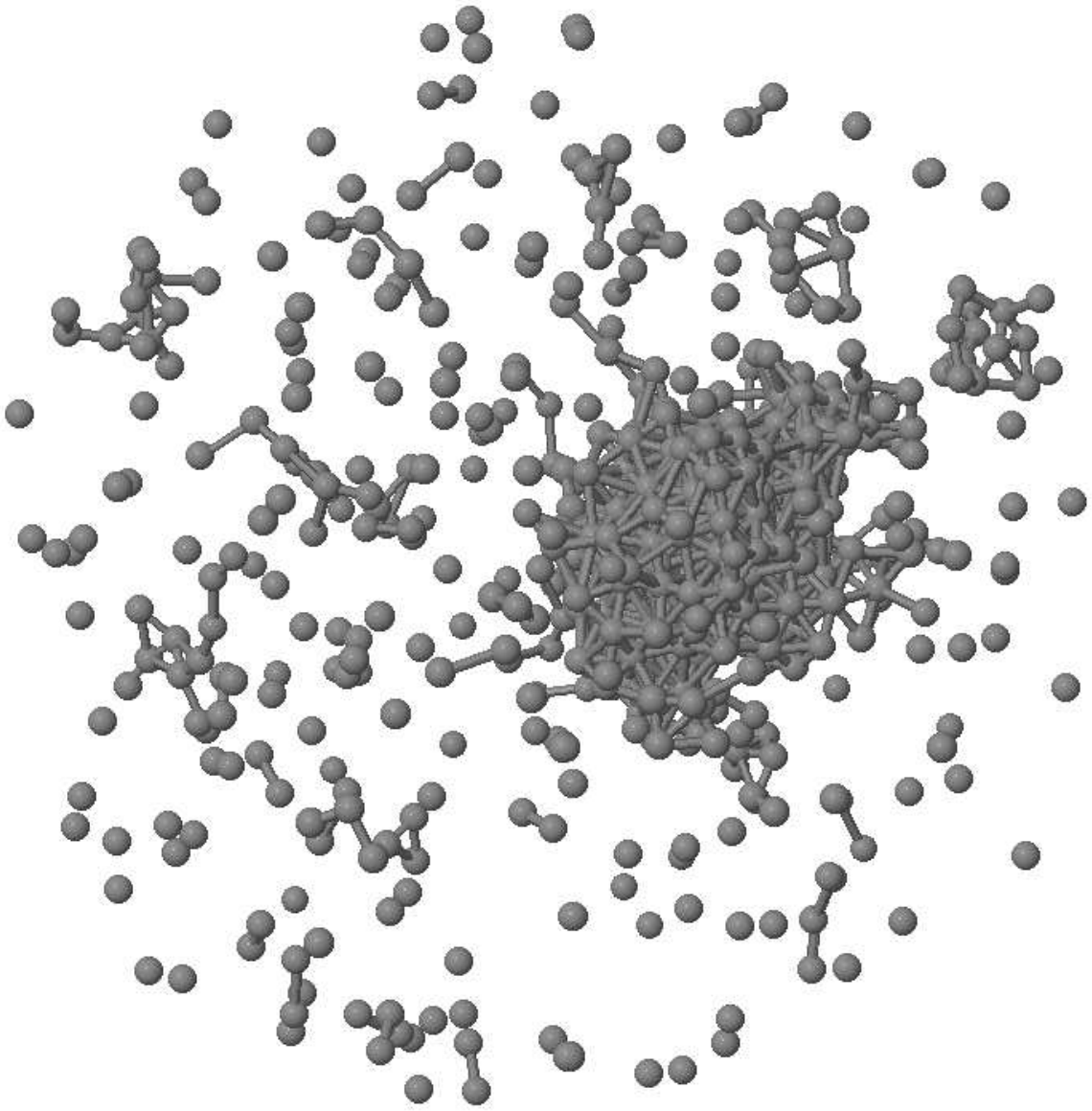

Figure 8. A realization of a Lennard-Jones simulation showing a drop (the large cluster at mid-height and towards the right) in equilibrium with a vapor (the monomers, dimers, trimers, etc. surrounding the drop). The gray spheres show the particles. Clusters are shown by particles connected with gray cylinders.

6. Coulomb effects and their elimination

So far, we have discussed liquid-vapor equilibria in terms of clusters, but without considering the Coulomb effects which are ever present in nuclei and nuclear clusters. We will consider these effects below.

The liquid drop model [11] considers nuclei as *charged* drops of a Van der Waals like fluid. As mentioned above, the experimental characterization of cold bulk nuclear matter can easily be achieved by setting the surface, symmetry, and Coulomb terms of the liquid drop expression to zero and retaining just the volume term. This, together

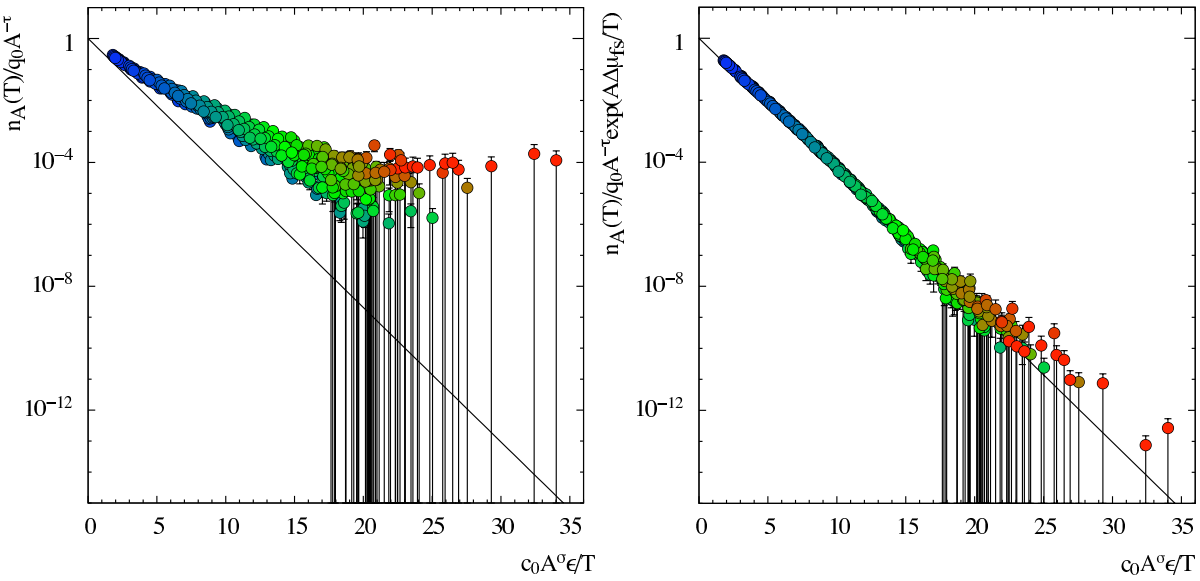

Figure 9. Cluster concentrations for the Lennard-Jones system for the liquid drop calculations without using the complement correction (left) and the liquid drop calculation with the complement (right). Here $c_0 = a_s$.

with the independent measurement of nuclear radii (inferable from the surface and Coulomb coefficients), defines the fundamental properties of cold bulk nuclear matter: its binding energy and density at saturation.

In this way, the Coulomb interaction is "eliminated" from the picture in order to dispose of what is properly perceived as a troublesome inessential divergence, while, for better or worse, it remains all pervasive in the experimental realm.

The experimental extension to higher temperatures is also hampered by the presence of the Coulomb interaction in a variety of ways.

In this section we consider the problem of the Coulomb interaction and the problem of the "container" for the vapor phase and present a simple and natural solution to both [27].

Many of the theoretical approaches to the Coulomb problem have been based upon numerical simulations of finite lattice systems [2, 3, 60]. In nuclei Coulomb effects become progressively more important with increasing A, Z and eventually, at $A \approx 60$ they reverse the surface trend prevailing at small A values. Above $A \approx 60$, the binding energy per nucleon reaches a maximum and then progressively decreases with increasing A.

One may wonder whether the role of the Coulomb interaction is merely that of decreasing the binding energy. The long range nature of this force may compel us to analyze its role in more detail in first order phase transitions. As will be shown below, the problems are quite serious and threaten our ability to define a true first order phase transition with any generality in the presence of such a force.

Let us introduce the Coulomb interaction in the problem of a drop and its vapor.

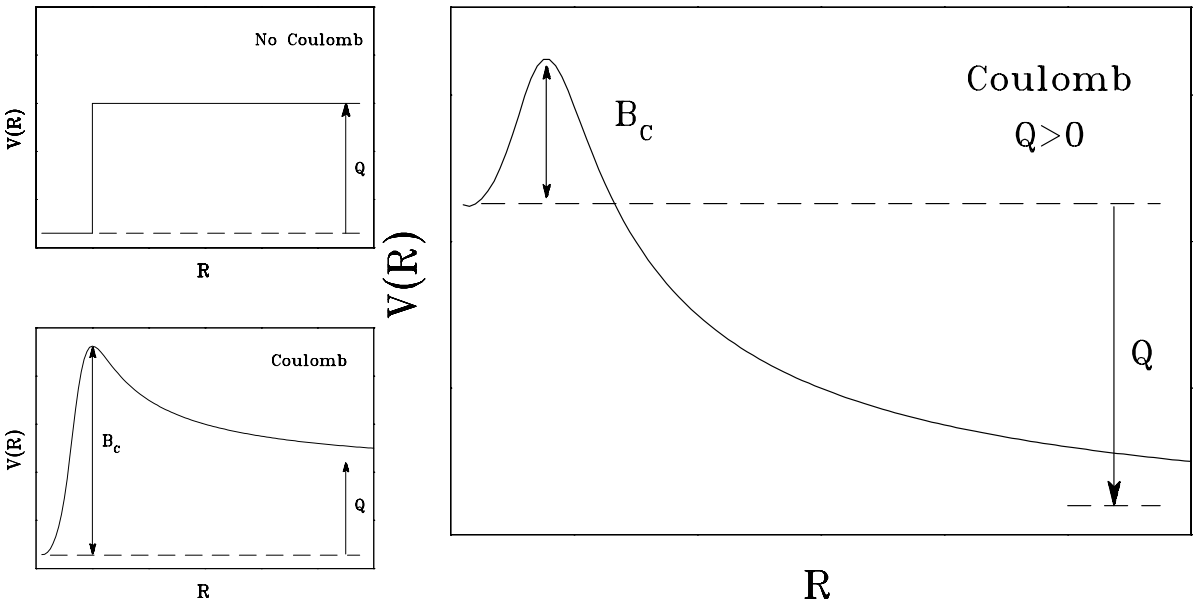

Figure 10. Top left panel: the schematic potential of an uncharged and bound particle ($Q < 0$) leaving a nucleus. Bottom left panel: the schematic potential of a bound charged particle. The charged particle must overcome a Coulomb barrier B_c in order to leave the nucleus. Right: The schematic potential of an unbound charged particle.

The Coulomb interaction can be split into three parts:

(i) the drop self-energy;

(ii) the drop-vapor interaction energy; and

(iii) the vapor self-energy.

The drop self energy, for a finite bound or metastable drop, is easily calculated and does not constitute a problem.

For the drop-vapor interaction, we consider a probe cluster which we can carry from the interior of the drop to infinity. The potential energy $V(r)$ experienced in the process depends upon the particle's charge/mass and is shown schematically in Fig. 10.

If the particle has zero charge (top panel of Fig. 10), a step is observed at the droplet radius equal to the particle binding energy. For charges greater than zero, a maximum $V(R_c) = B_c$ is observed at the approximate distance of the two droplets in contact at R_c. From there the potential decreases according to the Coulomb law and settles down at infinity to a value equal to the binding energy of the particle, Q.

In this case, where we assume that any particle of any size is bound ($Q < 0$) and we forget about problem (iii), there is no difficulty in defining a gas phase in equilibrium with the droplet at infinity constituted by particles of all sizes whose abundance is controlled by the respective binding energies in the standard way. The intervening Coulomb barrier B_c does not alter the equilibrium, although it may slow its achievement. In this case the vapor is constituted mainly of monomers and the coexistence pressure

described by the Clapeyron equation

$$\frac{dp}{dT} = \frac{\Delta H_e^m}{T\Delta V^m} \tag{42}$$

with ΔH_e^m suitably accounting for both surface and Coulomb terms, may be adequate to describe the liquid to vapor transition and coexistence.

Let us now consider the case in which the probe particle becomes unbound to the droplet above some Z value, due to the Coulomb interaction. Now the situation becomes as depicted in Fig. 10. In this case the droplet is not stable and the ground state of the system may consist of two or more pieces of the original drop at infinity. This is true already at $T = 0$. *Thus it is not possible to speak properly of this drop in statistical equilibrium with its vapor, since the drop itself is metastable.*

For a nucleus like gold, the ground state is at least as complicated as three fragments of approximately 60 nucleons at infinity. This "true" ground state is over one hundred MeV below the mass of the gold nucleus.

In any statistical calculation, at any reasonable temperature, one can expect a liquid-like phase consisting of a configuration similar to the true ground state in equilibrium with some vapor. A metastable gold-like drop is an immensely improbable configuration because of the great energy chasm mentioned above. The probability P of such a configuration can be surmised by the Boltzmann factor $P \propto \exp(-\Delta E/T)$, where ΔE is the energy difference between the metastable state and the ground state. For $\Delta E \approx 135$ MeV (which is approximately the value for Au and its true ground state) and a temperature of 4 MeV we obtain $P \approx e^{-34}$ or about 2×10^{-15}!

One might argue that our point is made from energetic rather than free energy F considerations and that it may in fact be incorrect. After all, equilibria work both ways, and typically one of the phases is at a lower energy than the other.

Let us consider, then, the transition from a condensed phase (liquid-like) to a dilute phase (vapor-like). For an infinitesimal isothermal transfer, the variation of the free energy must be zero

$$\Delta F = \Delta E - T\Delta S = 0 \tag{43}$$

where S is the entropy. As we go from liquid to vapor, $\Delta E > 0$ for a typical fluid, but this energy increase is compensated by an equivalent increase in entropy, due just to the increase in molar volume.

However, if ΔE is negative, due to the Coulomb effect, we need a <u>decrease</u> in entropy which is hardly compatible with expansion. The conclusion is that a statistical equilibrium first order phase coexistence and phase transition is <u>not definable</u> for any droplet that has unbound channels. Of course, the transition of the metastable droplet to its "true" complex ground state hardly qualifies as a statistical phase transition. Thus Coulomb effects seem truly devastating since they do not allow one to define nuclear phase transitions unambiguously.

However, there may be a partial solution to this difficulty. If we consider the emission of particles with a sizable charge, we notice that a large Coulomb barrier B_c is

present. For $T << B_c$ these channels may be considered effectively closed. Consequently the unbound channels may not play a role on a suitably short time scale. Then a phase transition may still be definable in an approximate way.

Let us consider now part 3) of the Coulomb energy, namely the vapor self energy. Obviously, the self energy diverges for an infinite amount of vapor. For a dilute vapor, we could consider a small portion such that the intrinsic self energy per nucleon is much less than the temperature T. Alternatively, we could consider a finite box containing a finite system. Unfortunately, at any distance smaller than infinity the result depends annoyingly on the size (and shape!!) of the container and on whether the drop is confined or not in a specified location of the container; a rather inelegant and non-general situation leading to confusing questions about true equilibrium. In any case, it is clear that overall, the Coulomb term makes the definition of phase coexistence and phase transition intractable and ill-posed. In other words, *any physical nuclear reaction, fragmentation or otherwise, does not reflect in any clear way an underlying phase transition.*

6.1. Marginalization of the Coulomb problem

A solution to these difficulties can be arrived at by asking a slightly different question: is there a way to experimentally characterize the nuclear phase transition as if the Coulomb interaction were not there?

As mentioned above, any attempt to define and characterize both phases in the presence of the Coulomb interaction depends (at the very least) on the shape and size of a confining volume applied from without. This is artificial and lacks a desirable generality. But nature actually provides this "confining volume" for us. Any particle trying to leave the nucleus is "boxed in" by a barrier (B_s) which depends on the particle under consideration and on the residual nucleus; i.e. the complement. The top of this potential barrier is close in shape to the potential of two objects, particle and complement, in near contact. The tops of these barriers are actually conditional saddle points [61], conditional in the sense that the mass asymmetry is considered frozen.

According to standard transition state theory [62, 63, 64] all these saddles are in statistical equilibrium with the droplet and the decay rates give direct information on their population which is controlled by the Boltzmann factor $\exp(-B_s/T)$. For large enough B_s the observed experimental abundances are directly related to first chance emission and thus to the transition state rates.

The barrier B_s is given by

$$\begin{aligned} B_s &= E^s_{\rm surface} - E^{gs}_{\rm surface} + E^s_{\rm Coulomb} - E^{gs}_{\rm Coulomb} \\ &= \Delta E_{\rm surface} + \Delta E_{\rm Coulomb} \end{aligned} \tag{44}$$

where: $E^s_{\rm surface}$ and $E^{gs}_{\rm surface}$ are the surface energies of the saddle and ground state respectively; $E^s_{\rm Coulomb}$ and $E^{gs}_{\rm Coulomb}$ are the Coulomb energies for the same two configurations; and the two ΔE terms are the difference between the saddle and ground state.

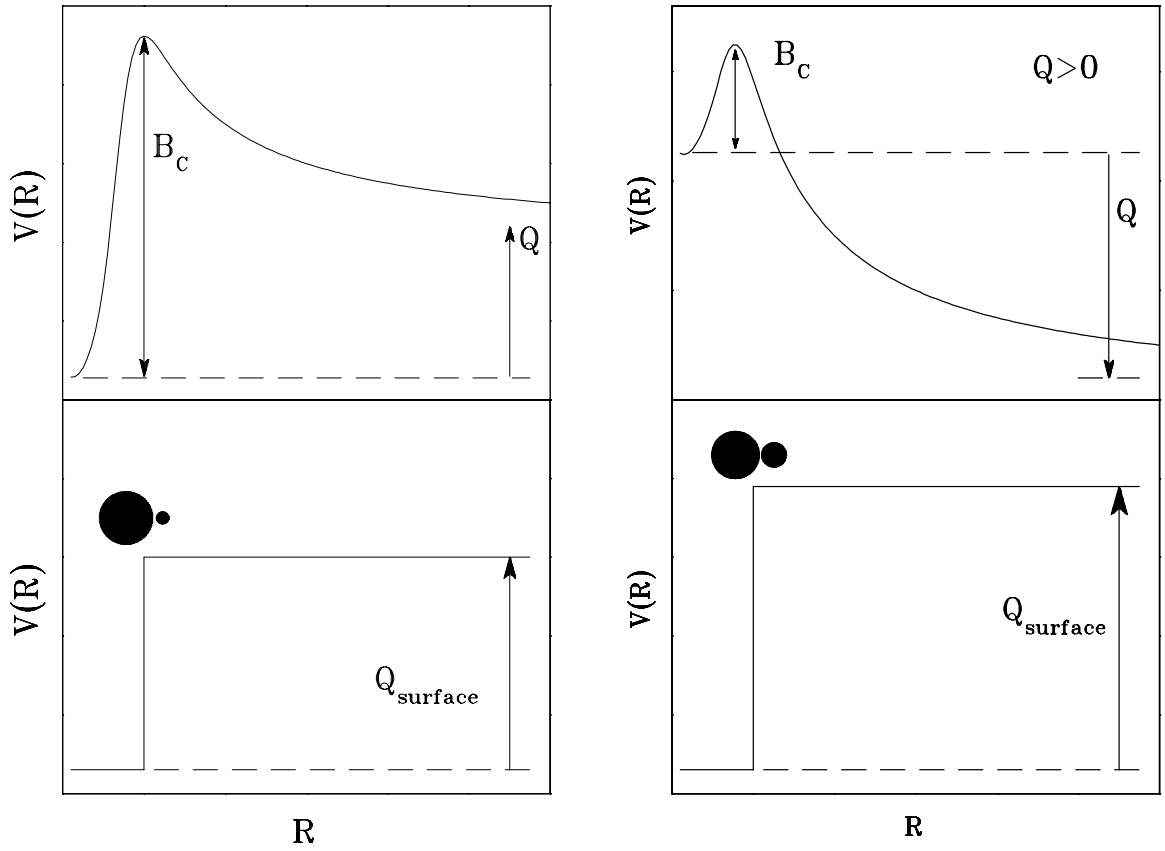

Figure 11. A schematic representation of the Coulomb correction when the emitted fragment is bound (left panels) and unbound (middle panels). In both cases one can remove the Coulomb energy of the saddle configuration and calculate the Q value using surface energies only (bottom panels). The resulting hypothetical gas will be composed of fragments that are bound to the droplet ($Q_{\rm surface} < 0$) for all fragment partitions.

The Coulomb energies can be easily estimated assuming a two touching spheres configuration for the saddle and one sphere configuration for the droplet as shown in Fig. 11. The decay rate R is then

$$R \propto \exp\left(-B_s\right) = \exp - \left(\Delta E_{\rm surface} + \Delta E_{\rm Coulomb}\right). \tag{45}$$

The Coulomb effects factor out, so we can correct the particle emission rates by dividing away the Boltzmann factor containing the Coulomb terms and be left with only the rates or particle abundances pertaining to the decay of an uncharged drop, for which all channels are bound by the extra surface energy given by

$$Q_{\rm surface} = E^s_{\rm surface} - E^{gs}_{\rm surface} \tag{46}$$

Figure 11 shows this schematically. This simple procedure allows us to set aside the Coulomb problem and related difficulties with boxes and equilibration.

These corrected rates are now proportional to the effective partial concentration of the hypothetical gas in equilibrium. This is a key result. We speak of a virtual gas phase because it is not and needs not be present. This picture of a free evaporation of a

droplet in vacuum neatly bypasses the need for a physical presence of the vapor. The resulting situation is very much that described by the Fisher droplet model [33, 34] for the composition of a saturated vapor in equilibrium with a liquid droplet.

Now the Fisher droplet model can be directly co-opted to describe the (first chance) fragment abundances of a nuclear physics experiment after correction for Coulomb effects. From it, it is easy to obtain the coexistence diagram for any nuclear system deprived of the Coulomb interaction [65, 66]. This is in the same spirit as in nuclear matter calculations in which neutrons and protons are considered as distinct particles, but without any Coulomb interaction.

7. Emission in vacuum and the virtual vapor

The previous section touched briefly upon the questions we now address in greater details. Those questions are: Where is the vapor? Does the nuclear system ever present itself at some time like a mixed phase system with the vapor being somehow constrained (as in lattice gas calculations [54, 26]), either statically or dynamically, to be in contact with the liquid phase? If so, how is the nuclear vapor restrained? If not, what is the meaning of vapor pressure, when clearly the system is freely decaying in vacuum against no pressure?

To answer these questions, we present a physical picture of fragment production from excited nuclei that will show: (a) how one can talk about coexistence without the vapor being present; and (b) why an equilibrium description, such as Fisher's theory, is relevant to the free vacuum decay of a multifragmenting system [25].

7.1. The virtual vapor

First, let us consider a liquid in equilibrium with its saturated vapor. At equilibrium, any particle evaporated by the liquid is restored on the average by the vapor bombarding it. In other words, the outward evaporation flux from the liquid to the vapor is matched by the inward condensation flux. This is true for any kind of evaporated particle. The vapor acts, as it were, like a mirror that reflects the evaporated particles back into the liquid.

One can probe the vapor by putting a detector in contact with it. However, since the outward and inward fluxes are identically the same, one might just as well put the detector in contact with the liquid itself. At equilibrium, the two measured fluxes must be the same. Therefore, *we do not need the vapor to be physically present in order to characterize it completely. We can just as well study the evaporation of the liquid and dispense with the surrounding saturated vapor. The vapor need not be there at all. One speaks in these situations of a "virtual vapor", realizing that first order phase transitions depend exclusively upon the intrinsic properties of the two phases, and not on their interaction.* Of course, if the vapor is not there to restore the emitting system with its return flux, evaporation will proceed and the system will cool.

This naturally suggests the study of the emission of fragments from an excited nucleus since the nucleus is a small drop of nuclear liquid evaporating in vacuum; i.e. emitting fragments in vacuum.

Next, we specifically address fragment emission from an excited nucleus with a time-honored assumption which we do not justify other than through the clarification it brings to the experimental picture: we assume (just as in compound nuclear decay [14]) that, after any prompt emission in the initial phase of the collision, the resulting system relaxes in shape and density and thermalizes *on a time scale shorter than its thermal decay*. At this point the excited nucleus emits particles in vacuum, *according to standard statistical decay rate theory*. In this picture there is no surrounding vapor, no confining box; there is no need for either. By studying the outward flux of the *first* fragments emitted (first chance emission), we can study the nature of the vapor even when it is absent (the *virtual* vapor) because of the equivalence of the evaporation and condensation fluxes of a liquid in equilibrium with its saturated vapor.

Quantitatively, the concentration $n_A(T)$ of any species A in the vapor is related to the corresponding decay rate $R_A(T)$ (or to the decay width Γ_A) from the nucleus by matching the evaporation and condensation fluxes

$$R_A(T) = \frac{\Gamma_A(T)}{\hbar} \simeq n_A(T) \left\langle v_A(T) 4\sigma_{\rm inv}(v_A) \right\rangle , \tag{47}$$

where $v_A(T)$ is the thermal velocity of the species A (of order $\sqrt{T/A}$) crossing the nuclear interface represented by the cross section $\sigma_{\rm inv}$ (of order $A_0^{2/3}$ where A_0 is the mass number of the evaporating nucleus). The temperature T of the equilibrated, excited nucleus when the first fragment is emitted can be estimated by the thermometric equation of a Fermi gas and the calorimetrically mesaured excitation energy E^*

$$T = \sqrt{E^*/a} \tag{48}$$

allowing for a weak dependence of a on T [67, 68], and remembering that the system is most likely still in the Fermi strong degeneracy regime (where the temperature is much less than the Fermi energy: $T \ll \varepsilon_F$).

This is the fundamental and simple connection between Eq. (47), the (compound nucleus) decay rate, and Eq. (20). In the latter, one immediately recognizes in the exponential the canonical expansion of the standard compound nucleus decay rate, namely the Boltzmann factor $\exp(-B/T)$ where B is the emission barrier which in Eq. (20) is written with its surface factor isolated from all other components, e.g. Coulomb [27], symmetry, finite size [26], etc. Thus, the vapor phase in equilibrium can be completely characterized in terms of the decay rate.

The physical picture described above is valid instantaneously, but not globally. The result of a global or successive evaporation in vacuum leads to abundances of various species of emitted fragments that arise from a continuum of systems at different temperatures [69]. This leads to complications in various thermometers: kinetic energy, isotope ratios, etc. Our way to avoid this complication is to consider only fragments that are emitted very rarely so that, if they are not emitted first, they are effectively

not emitted at all. In other words, we consider only fragments that by virtue of their large surface energy (and high charge), have a high emission barrier.

It is worth noting that the rapidly increasing Coulomb barrier with fragment charge Z strongly enhances this effect. Thus a lower cut-off of about $Z = 6$ is used.

8. Experimental fragment distributions

Using the above physical picture and prescriptions to deal with the Coulomb force and finite size effects, the fragment distributions from two types of experiments are analyzed in this work.

One type of experiment gives rise to a standard "compound nucleus." A compound nucleus is formed when one nucleus impacts another nucleus and the two combine to form a single, compound excited nucleus. The nucleon number and charge of the compound nucleus is just the sum of the nucleon number and charge of the two colliding nuclei. Energy and angular momentum can easily be calculated [70].

The other type of experiment deals with what is loosely called "multifragmentation" [71, 72, 73, 74, 75, 76, 77, 78, 79, 65, 66, 9] In a multifragmentation experiment, one nucleus is accelerated to a high velocity and impacts another nucleus. In the multifragmentation experiments considered here, one of the colliding nuclei is much larger than the other. The collision between nuclei in multifragmentation experiments is more violent than the collisions in the compound nucleus experiments and instead of the two nuclei combining to form a compound nucleus, the larger of the two nuclei has nucleons ejected during the collision leaving an excited remnant with a smaller nucleon number and charge than the initial nucleus. The more violent the collision, the greater the excitation of the remnant, but the smaller the nucleon number and charge of the remnant. This remnant can be considered as an equilibrated compound nucleus which thermally decays by emitting nucleons and clusters. Analyses similar to that presented here has been performed previously [80, 65, 66]. However, those efforts did not properly take into account the Coulomb force and finite size effects.

8.1. Analysis

For both types of experiments it is assumed that the collisions produce an excited, equilibrated remnant (hereafter the compound nucleus is also referred to as a remnant) of radius $r_{\rm r}$ consisting of $A_{\rm r}$ nucleons ($Z_{\rm r}$ protons and $N_{\rm r}$ neutrons) at excitation energy $E^*_{\rm r}$ with angular momentum $\left|\vec{L}\right|$. This is the initial state of the system, an excited heavy nucleus that will emit neutrons and charged particles.

The analysis of the data leads to the characterization of the decaying compound nucleus or remnant in terms of its mass $A_{\rm r}$, charge Z, excitation energy $E^*_{\rm r}$, angular momentum $\left|\vec{L}\right|$ and of the yield $Y\left(Z_{\rm r}, A_{\rm r}\right)$ of emitted fragments of charge $Z_{\rm f}$ and mass $A_{\rm f}$ (the fragment mass number is corrected for secondary decay). The excitation energy is transformed into a temperature via the Fermi gas approximation [67, 68].

Contributions to the free energy of fragment formation that arise from the angular momentum of the system are calculated. The data are then analyzed according to the procedures illustrated above. Complete and in depth details of this analysis can be found in reference [81].

The data from six different reactions (listed in Table 4) and three different experiments were used and over 500 data points were fit with three (for the compound nuclear data sets) or four (for the multifragmentation data sets) free parameters per reaction (there were, on average, nearly 23 data points per free parameter). Charges from $6 \leq Z_{\rm f} \leq 25$ and excitation energies of 1.08 AMeV $\leq E^*_{\rm r} \leq$ 4.75 AMeV were used in the analysis.

Table 4 shows the results for T_c from all the experiments. These values agree with each other to within 3% and give an estimate of the critical temperature of bulk nuclear matter as $T_c = 17.9 \pm 0.4$ MeV. This value agrees well with theoretical predictions [82, 83, 84, 7, 85].

Table 4. Estimates of the critical temperature from six different reactions.

Reaction	T_c (MeV)
^{58}Ni+^{12}C$\rightarrow^{70}$Se	18.4 ± 0.3
^{64}Ni+^{12}C$\rightarrow^{76}$Se	18.0 ± 0.2
1 AGeV ^{84}Kr+^{12}C	17.5 ± 0.2
1 AGeV ^{139}La+^{12}C	18.3 ± 0.2
1 AGeV ^{197}Au+^{12}C	17.7 ± 0.1
1 GeV/c π+^{197}Au	17.26 ± 0.02

Plotting the scaled ratio of the yields of a given fragment $Y\left(Z_{\rm r}, A_{\rm r}\right)$ as a function of $a_s A^\sigma \varepsilon / T$ collapses the measured fragment yields for any $A_{\rm f}$ and $E^*_{\rm r}$ onto a single curve [81]. This is shown in Figure 12. This figure shows that all the data from the six reactions can be collapsed onto a single curve. The curve is, for all intents and purposes, the liquid-vapor coexistence curve of bulk nuclear matter since the effects of finite size, the Coulomb force, angular momentum and isospin have all been accounted for and scaled out.

8.1.1. Constructing the phase diagram The above analysis provides us with the critical temperature of nuclear matter and direct information about the liquid-vapor coexistence curve. With T_c determined and additional work, it is possible to determine the coexistence curve of nuclear matter that completely maps the liquid-vapor phase diagram in (T,ρ,p).

The first step is to determine the coexistence curve in reduced units:

$$\frac{p}{p_c}, \frac{\rho}{\rho_c} \text{ and } \frac{T}{T_c}. \tag{49}$$

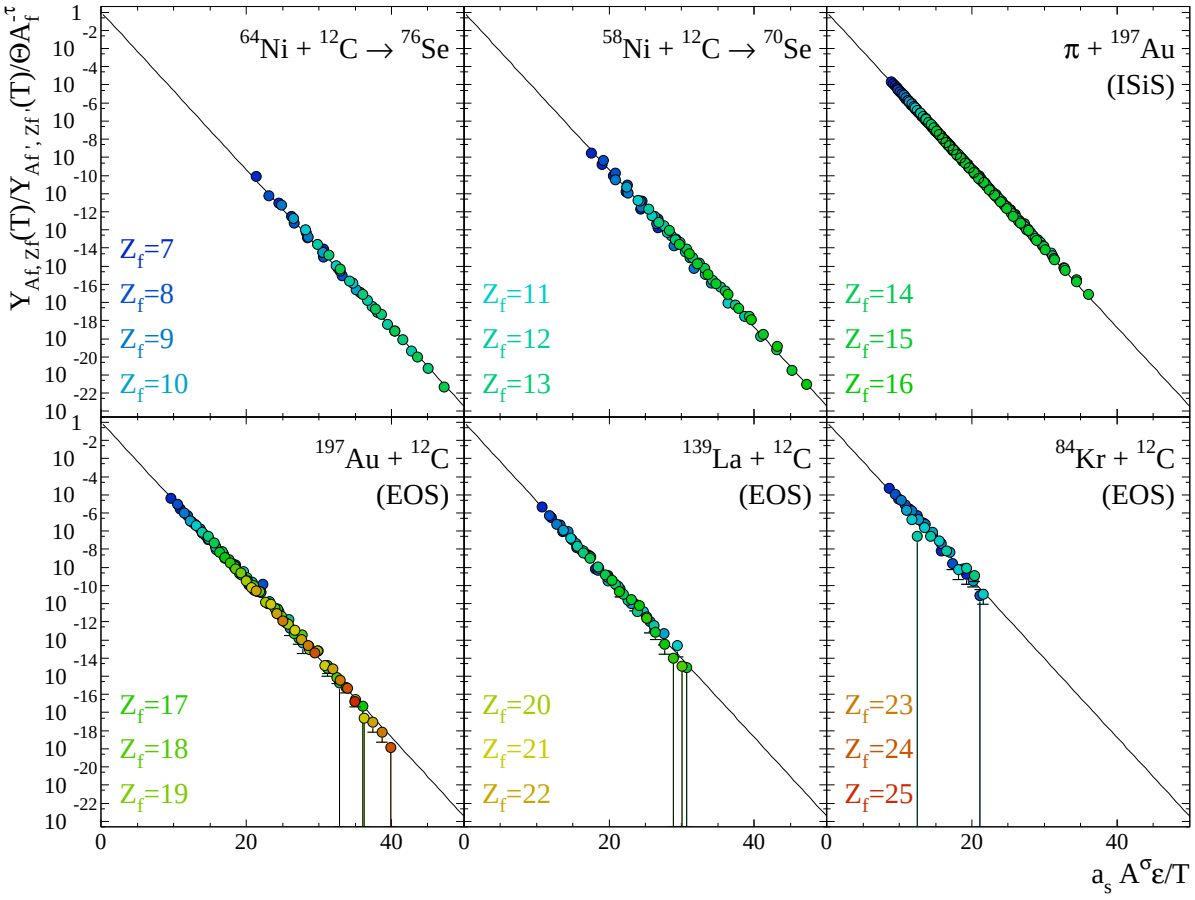

Figure 12. The scaled charge yields for all six reactions. Over 500 points are collapsed onto a single curve which describes the behavior of bulk nuclear matter. The color of the points show the charge of the fragments. The solid line shows the liquid-vapor coexistence curve of bulk nuclear matter. Here Θ is an effective chemical potential that depends on the effects of finite size, the Coulomb force, angular momentum and isospin. See reference [81] for further details.

We recall that in Fisher's theory the formation of clusters (or fragments) exhausts all non-idealities of the vapor, so that the pressure and density can be obtained by simple sums. The pressure is

$$p = T\sum_A n_A(T) = T\sum_A q_0 A^{-\tau}\exp\left(-\frac{a_s A^{\sigma}\varepsilon}{T}\right) \tag{50}$$

and at the critical point

$$p_c = T_c\sum_A n_A(T_c) = T_c q_0\sum_A A^{-\tau}. \tag{51}$$

The density is given by

$$\rho = \sum_A A n_A(T) = \sum_A q_0 A^{1-\tau}\exp\left(-\frac{a_s A^{\sigma}\varepsilon}{T}\right) \tag{52}$$

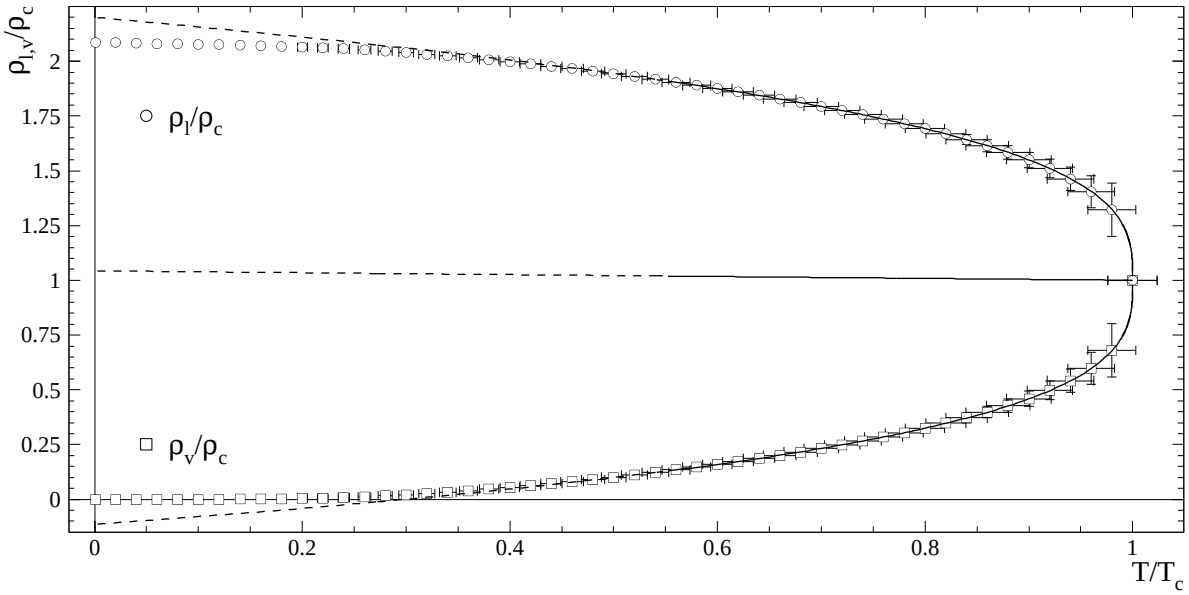

Figure 13. The reduced density-reduced temperature coexistence curve for bulk nuclear matter. Empty squares show the vapor branch. Empty circles show the liquid branch. Solid curves show the results of the fit to the vapor branch. Dotted curves show the extrapolation of that fit. The dashed line shows the extrapolation of the law of rectilinear diameter. See text for details.

and at the critical point

$$\rho_c = \sum_A A n_A(T_c) = q_0 \sum_A A^{1-\tau}. \tag{53}$$

Using the reduced quantities removes the unknown normalization q_0. All other quantities in the above sums are known. The errors associated with T_c, τ and σ are propagated to generate errors on the reduced quantities.

8.1.2. Reduced density The empty squares in Figure 13 shows the vapor branch of the ρ-T phase diagram of nuclear matter, albeit in reduced form. The empty circles in Figure 13 show the liquid branch which was determined as follows. First, Guggenheim's universal function describing the reduced $\rho_{\rm l,v}/\rho_c$-T/T_c phase diagram [23]

$$\frac{\rho_{\rm l,v}}{\rho_c} = 1 + d_1\varepsilon \pm d_\beta \varepsilon^\beta \tag{54}$$

was fit to the empty squares on Figure 13 from $0.55T_c \leq T \leq T_c$ which is roughly the range over which Guggenheim's function describes dozens of fluids: from the triple point to the critical point. Here the critical exponent β is [33, 34, 45]

$$\beta = \frac{\tau - 2}{\sigma} = 0.3265 \pm 0.0001 \tag{55}$$

and d_1 and d_β are left as fit parameters. The vapor branch is described by the Eq. (54) with the minus sign and the liquid branch is described by the Eq. (54) with the plus sign. The solid curve on Figure 13 shows the results from the fitting procedure.

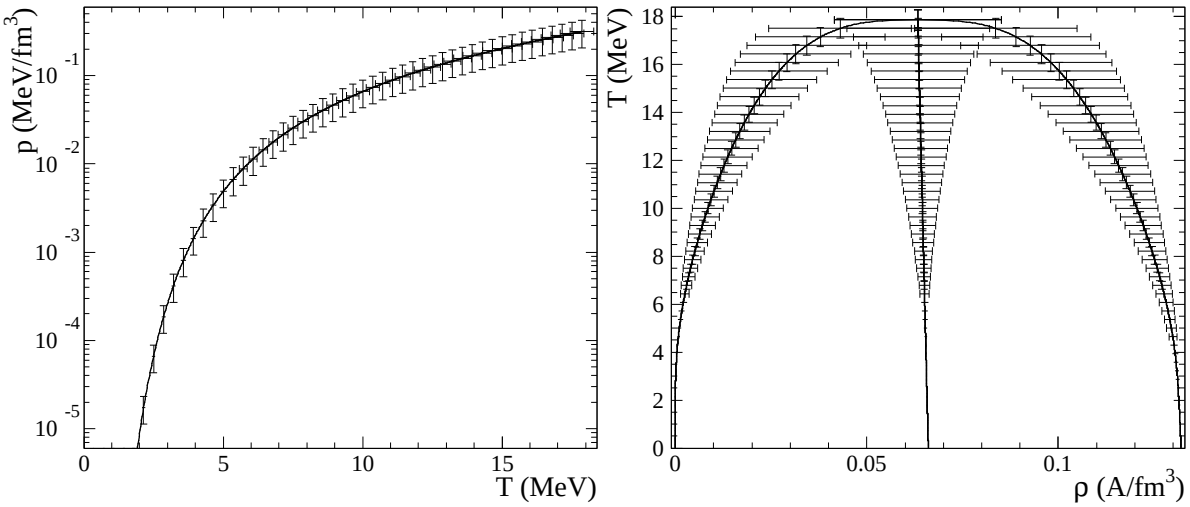

Figure 14. Left: The pressure-temperature coexistence curve for bulk nuclear matter. Right: The temperature-density coexistence curve for bulk nuclear matter. Errors are shown for selected points to give an idea of the error on the entire coexistence curve.

Dotted curves on Figure 13 show extrapolations for $T < 0.55T_c$. The extrapolation for the vapor branch shows unphysical behavior with $\rho_v/\rho_c < 0$ for $T/T_c < 0.25$, thus some care must be taken when determining the $\rho_{\rm l}/\rho_c$-T/T_c coexistence curve at low temperatures. The $\rho_{\rm v}/\rho_c$-T/T_c coexistence curve at low temperatures has already been determined from equations (52) and (53).

To determine the liquid branch of the coexistence curve for low temperatures we start with the law of rectilinear diameter which is

$$\frac{\rho_l + \rho_v}{2\rho_c} = 1 + d_1\varepsilon. \tag{56}$$

We extrapolate this linear function in ε from $T = 0.55T_c$ to $T = 0$. This is shown by the dashed line in Figure 13. We then use that extrapolation and the values of ρ_v/ρ_c computed via the sums in equations (52) and (53) (open circles on Figure 13) to solve for ρ_l/ρ_c at low temperatures by "reflecting" them about the line defined by Eq. (56). Thus

$$\frac{\rho_{\rm l}}{\rho_c} = 2 + 2d_1\varepsilon - \frac{\rho_v}{\rho_c}. \tag{57}$$

The results are shown by empty squares on Figure 13. The error bars on ρ_l/ρ_c are equal to the error bars on ρ_v/ρ_c.

8.1.3. Density To obtain a $\rho_{\rm l,v}$-T coexistence curve in a non-reduced form (e.g. temperature in units of MeV and density in units of nucleons per cubic fermi) we first multiply the temperature axis by T_c. Errors on the temperature scale are then given by:

$$\delta T = \delta T_c \left(\frac{T}{T_c}\right). \tag{58}$$

To determine the density in units of nucleons per cubic fermi we note that at $T = 0$ the density of nuclear matter should be approximately the density observed in unexcited nuclei. Using the value of $r_0 = 1.2181$ fm the density of nuclear matter at $T = 0$ is

$$\rho_l\left(T=0\right) = \frac{3}{4\pi r_0^3} \approx 0.132A/\mathrm{fm}^3. \tag{59}$$

That value sets the scale on the density axis. The results are shown in Figure 14 and we obtain a critical density value of $\rho_c = 0.06 \pm 0.02$ A/fm^3 which agrees well with theoretical efforts [83, 84, 7, 85].

8.1.4. Pressure To determine the coexistence curve for pressure as a function of temperature we again start with the reduced quantities and obtain p/p_c as a function of T/T_c by performing the sums in equations (50) and (51). We then determine the value of p_c from the compressibility at the critical point which is defined as

$$Z_c = \frac{p_c}{\rho_c T_c}. \tag{60}$$

For fluids this is a universal quantity and is $Z_c = 0.277 \pm 0.004$ [81]. Combining equations (51), (53) and (60) one sees that the compressibility at the critical point is just a ratio of two Riemann ζ-functions [86, 87]

$$Z_c = \frac{\zeta\left(\tau-1\right)}{\zeta\left(\tau\right)} = 0.276. \tag{61}$$

However, using the error on τ gives $Z_c = 0.28 \pm 0.01$. We use this value of Z_c in combination with the values of T_c and ρ_c determined above to obtain a value for the pressure at the critical point of 0.3 ± 0.1MeV/fm^3 which agrees well with theoretical efforts [84, 85]. Here the error arise from the errors on T_c and ρ_c. Now to obtain the pressure in units of MeV/fm^3 we merely multiply p/p_c by the value of p_c obtained above. The error on the pressure is given by

$$\delta p = \delta p_c \frac{p}{p_c}. \tag{62}$$

Figure 14 shows these results.

9. Conclusion

Our goal in this paper was to identify and employ an experimental method applicable to suitably chosen nuclear reactions in order to extract that liquid-vapor phase diagram of infinite, uncharged, symmetric nuclear matter. The usual thermodynamical methods being obviously not accessible, we concentrated on the possibility of using cluster mass distributions at various temperatures and analyzing them according to Fisher's cluster theory. This method has two advantages. On one hand it can be tested against models where the phase diagram is independently known. On the other, strongly thermalized nuclear reactions produce clusters that are readily measured.

A Fisher analysis of the cluster distributions obtained for equilibrated Ising and Lennard-Jones simulations showed that we could indeed recover satisfactorily the phase diagrams of both systems.

The application to nuclei, however, presented three additional difficulties: the finite size of nuclear systems, the presence of the Coulomb force, and the absence of a stationary vapor phase coexisting with the liquid.

The finite size problem was solved by a very simple and effective approach, the complement approach. The free energy associated with the extraction of a cluster from a finite drop rather than from the infinite liquid led us to a generalization of the Fisher formalism. By means of it we could fit the cluster distributions in equilibrium with a finite drop and extract the relevant parameters pertaining to the infinite system. This was tested on Ising and Lennard-Jones vapors in equilibrium with finite drops with excellent results.

The Coulomb effects were eliminated by considering the cluster decay rates of a charged system according to the transition state method. The Coulomb term could be factored out and divided away leaving a corrected decay rate for the corresponding uncharged system. This rate can be directly related to the concentration of the vapor in equilibrium.

Finally, the lack of a stationary vapor phase was obviated by realizing that the thermal decay rates of the uncharged system could be directly related to the corresponding concentrations of the saturated vapor. Having developed and tested in so far as possible this systematic approach, we proceeded to apply it to a series of nuclear reactions, low energy compound nucleus decay and higher energy multifragmentation.

Low energy compound nuclear reactions were particularly important because the mass, charge, excitation energy and angular momentum of the decaying system could be easily determined.

The resulting analysis led to a very consistent set of parameters, which allowed us to achieve the reconstruction of the desired phase diagram.

10. Acknowledgments

This work was performed by by Lawrence Berkeley National Laboratory and was supported by the Director, Office of Energy Research, Office of High Energy and Nuclear Physics, Division of Nuclear Physics, of the U.S. Department of Energy under Contract No. DE-AC02-05CH11231.

This work also performed under the auspices of the U.S. Department of Energy by Lawrence Livermore National Laboratory under Contract DE-AC52-07NA27344.

References

[1] Jörg Aichelin. “quantum” molecular dynamics—a dynamical microscopic n-body approach to investigate fragment formation and the nuclear equation of state in

heavy ion collisions. *Physics Reports*, 202(5):233–260, Apirl 1991.

[2] J. P. Bondorf, A. S. Botvina, A. S. Iljinov, I. N. Mishustin, and K. Sneppen. Statistical multifragmentation of nuclei. *Physics Reports*, 257(3):133–221, June 1995.

[3] D. H. E. Gross. Microcanonical thermodynamics and statistical fragmentation of dissipative systems. the topological structure of the n-body phase space. *Physics Reports*, 279(3):119–201, January 1997.

[4] L. G. Moretto, K. Tso R. Ghetti, L. Phair, and G. J. Wozniak. Reducibility and thermal scaling in nuclear multifragmentation. *Physics Reports*, 287(3):249–336, August 1997.

[5] J. Richert and P. Wagner. Microscopic model approaches to fragmentation of nuclei and phase transitions in nuclear matter. *Physics Reports*, 350(1):1–92, August 2001.

[6] N. Sator. Clusters in simple fluids. *Physics Reports*, 376(1):1–39, March 2003.

[7] P. Chomaz, M. Colonna, and J. Randrup. Nuclear spinodal fragmentation. *Physics Reports*, 389(5):263–440, January 2004.

[8] C.B. Das, S. Das Gupta andW.G. Lynch, A.Z. Mekjian, and M.B. Tsang. The thermodynamic model for nuclear multifragmentation. *Physics Reports*, 406(1):1–47, January 2005.

[9] V.E. Viola, K. Kwiatkowski, L. Beaulieu, D.S. Bracken, H. Breuer, J. Brzychczyk, R.T. de Souza, D.S. Ginger, W-C. Hsi, R.G. Korteling, T. Lefort, W.G. Lynch, K.B. Morley, R. Legrain, L. Pienkowski, E.C. Pollacco, E. Renshaw, A. Ruangma, M.B. Tsang, C. Volant, G. Wang, S.J. Yennello, and N.R. Yoder. Light-ion-induced multifragmentation: The isis project. *Physics Reports*, 434(1):1–46, November 2006.

[10] B. Borderie and M.F. Rivet. Nuclear multifragmentation and phase transition for hot nuclei. *Progress in Particle and Nuclear Physics*, 61(2):551–601, October 2008.

[11] C. F. v. Weizsäcker. Zur theorie der kernmassen. *Zeitschrift Für Physik A Hadrons and Nuclei*, 96(7):431–458, July 1935.

[12] W. D. Myers and W. J. Swiatecki. Nucleus-nucleus proximity potential and superheavy nuclei. *Physical Review C*, 62(4):044610.1–044610.7, September 2000.

[13] G. Royer and C. Gautier. Coefficients and terms of the liquid drop model and mass formul. *Physical Review C*, 73(6):067302.1–067302.4, June 2006.

[14] V. Weisskopf. Statistics and nuclear reactions. *Physical Review*, 52(4):295–303, August 1937.

[15] N. Bohr and J. A. Wheeler. The mechanism of nuclear fission. *Physical Review*, 56(5):426–450, September 1939.

[16] E.W. Lemmon, M.O. McLinden, and D.G. Friend. *"Thermophysical Properties of Fluid Systems" in NIST Chemistry WebBook NIST Standard Reference Database.* Number 69. National Institute of Standards and Technology, Gaithersburg MD 20899, June 2005.

[17] P. Möller, J. R. Nix, W. D. Myers, and W. J. Swiatecki. Nuclear ground-state masses and deformations. *Atomic Data and Nuclear Data Tables*, 59(2):185–381, March 1995.

[18] V. M. Strutinsky. Microscopic calculations of the nucleon shell effects in the deformation energy of nuclei. *Arkiv för Fysik*, 36:629, 1967.

[19] V. M. Strutinsky. Shell effects in nuclear masses and deformation energies. *Nuclear Physics A*, 95(1):420–442, April 1967.

[20] V. M. Strutinsky. "shells" in deformed nuclei. *Nuclear Physics A*, 122(1):1–33, December 1968.

[21] J. D. van der Waals. *Over de Continuiteit van den Gas en Vloeistoftoestand*. doctoral physics, Leiden University, Niels Bohrweg 2, 2333 CA Leiden, June 1873.

[22] J. E. Finn, S. Agarwal, A. Bujak, J. Chuang, L. J. Gutay, A. S. Hirsch, R. W. Minich, N. T. Porile, R. P. Scharenberg, B. C. Stringfellow, and F. Turkot. Nuclear fragment mass yields from high-energy proton-nucleus interactions. *Physical Review Letters*, 49(18):1321–1325, November 1982.

[23] E. A. Guggenheim. The principle of corresponding states. *Journal of Chemical Physics*, 13(7):253–262, July 1945.

[24] E. A. Guggenheim. *Thermodynamics*. North-Holland Elsevier Science Publishers B. V., Sara Burgerhartstraat 25, P. O. Box 211, 1000 AE Amsterdam, The Netherlands, fourth impression (paper back) edition, 1993.

[25] L. G. Moretto, J. B. Elliott, and L. Phair. Compound nuclear decay and the liquid-vapor phase transition: A physical picture. *Physical Review C*, 72(6):064605.1–064605.6, December 2005.

[26] L. G. Moretto, K. A. Bugaev, J. B. Elliott, R. Ghetti, J. Helgesson, and L. Phair. The complement: A solution to liquid drop finite size effects in phase transitions. *Physical Review Letters*, 94(20):202701.1–202701.4, May 2005.

[27] L. G. Moretto, J. B. Elliott, and L. Phair. Resistible effects of coulomb interaction on nucleus-vapor phase coexistence. *Physical Review C*, 68(6):061602(R).1–061602(R).5, December 2003.

[28] L. Beaulieu, L. Phair, L. G. Moretto, and G. J. Wozniak. z-dependent barriers in multifragmentation from poissonian reducibility and thermal scaling. *Physical Review Letters*, 81(4):770–773, July 1998.

[29] L. G. Moretto and G. J. Wozniak. The categorical space of fission. *Pramana - Journal of Phyiscs*, 33(1):209–253, July 1989.

[30] L. G. Moretto and G. J. Wozniak. Thermal and statistical properties of nuclei and nuclear systems. In C. Détrazand P. Kienle, editor, *Nuclear Collisions from the Mean-Field into the Fragmentation Regime*, pages 249–312, Amsterdam, July 1991. North-Holland Elsevier Science Publishers B. V.

[31] J. E. Mayer and M. G. Mayer. *Statistical Mechanics*. John Wiley, New York, 1940.

[32] J. Frenkel. *Kinetic Theory of Liquids*. Oxford University Press, London, 1946.

[33] M. E. Fisher. The theory of condensation and the critical point. *Physics (Long Island City, NY)*, 3(5):255–283, 1967.

[34] M. E. Fisher. The theory of equilibrium critical phenomena. *Reports on Progress in Physics*, 30(2):615–730, July 1967.

[35] T. D. Lee and C. N. Yang. Statistical theory of equations of state and phase transitions. ii. lattice gas and ising model. *Physical Review*, 87(3):410–419, August 1952.

[36] C. N. Yang and T. D. Lee. Statistical theory of equations of state and phase transitions. i. theory of condensation. *Physical Review*, 87(3):404–409, August 1952.

[37] H. Gould and J. Tobochnik. *An Introduction to Computer Simulation Methods - Applications to Physical Systems*. Addison-Wesley Publishing Company, Inc., Reading, Massachusetts, second edition edition, 1996.

[38] A. Coniglio and W. Klein. Clusters and ising critical droplets: a renormalisation group approach. *Journal of Physics A: Mathematical and General*, 13(8):2775–2780, August 1980.

[39] J. Kertész. Existence of weak singularities when going around the liquid-gas critical point. *Physica A*, 161(1):58–62, November 1989.

[40] D. Stauffer and A. Aharony. *Introduction to Percolation Theory*. Taylor & Francis Inc., 325 Chestnut Street, 8th Floor, Philidelphia PA 19106, revised second eddition edition, 2001.

[41] A. Z. Panagiotopoulos. Direct determination of phase coexistence properties of fluids by monte carlo simulation in a new ensemble. *Molecular Physics: An International Journal at the Interface Between Chemistry and Physics*, 61(4):813–823, July 1987.

[42] T. L. Hill. Molecular clusters in imperfect gases. *Journal of Chemical Physics*, 23(4):617–622, November 1953.

[43] C. M. Mader, A. Chappars, J. B. Elliott, L. G. Moretto, L. Phair, and G. J. Wozniak. The three-dimensional ising model and its fisher analysis: A paradigm of liquid-vapor coexistence in nuclear multifragmentation. *Physical Review C*, 68(6):064601.1–064601.6, December 2003.

[44] P. Butera and M. Comi. Critical universality and hyperscaling revisited for ising models of general spin using extended high-temperature series. *Physical Review B*, 65(14):144431.1–144431.14, April 2002.

[45] M. Campostrini, A. Pelissetto, P. Rossi, and E. Vicari. 25th-order high-temperature expansion results for three-dimensional ising-like systems on the simple-cubic lattice. *Physical Review E*, 65(6):066127.1–066127.19, June 2002.

[46] L. G. Moretto, J. B. Elliott, P. T. Lake, and L. Phair. The curvature correction paper. *in progress*, 2011.

[47] K. Okunishi and T. Nishino. Kramers-wannier approximation for the 3d ising model. *Progress Theoretical Physics*, 103(3):541–548, January 2000.

[48] Jeffrey J. Potoff and Athanassios Z. Panagiotopoulos. Critical point and phase behavior of the pure fluid and a lennard-jones mixture. *Journal of Chemical Physics*, 109(24):10914.1–10914.7, December 1998.

[49] J. K. Johnson, J. A. Zollweg, and K. E. Gubbins. The lennard-jones equation of state revisited. *Molecular Physics*, 78(3):591–618, February 1993.

[50] M. Schmidt, R. Kusche, T. Hippler, J. Donges, W. Kronmüller, B. von Issendorff, and H. Haberland. Negative heat capacity for a cluster of 147 sodium atoms. *Physical Review Letters*, 86(7):1191–1194, February 2001.

[51] B. Krishnamachari, J. McLean, B. Cooper, and J. Sethna. Gibbs-thomson formula for small island sizes: Corrections for high vapor densities. *Physical Review B*, 54(12):8899–8907, September 1996.

[52] N. B. Wilding. Critical-point and coexistence-curve properties of the lennard-jones fluid: A finite-size scaling study. *Physical Review E*, 52(1):602–611, July 1995.

[53] J. R. Heringa and H. W. J. Blöte. Geometric symmetries and cluster simulations. *Physica A: Statistical and Theoretical Physics*, 254(1):156–163, May 1998.

[54] J. B. Elliott, L. G. Moretto, and L. Phair. Saturated vapor properties and scaling in the lattice gas model. *Physical Review C*, 71(2):024607.1–024607.5, February 2005.

[55] A. E. Ferdinand and M. E. Fisher. Bounded and inhomogeneous ising models. i. specific-heat anomaly of a finite lattice. *Physical Review*, 185(2):832–846, September 1969.

[56] D. P. Landau. Finite-size behavior of the ising square lattice. *Physical Review B*, 13(7):2997–3011, April 1976.

[57] D. P. Landau. Finite-size behavior of the simple-cubic ising lattice. *Physical Review B*, 14(1):255–262, July 1976.

[58] A. M. Ferrenberg and D. P. Landau. Critical behavior of the three-dimensional ising model: A high-resolution monte carlo study. *Physical Review B*, 44(10):5081–5091, September 1991.

[59] L. Onsager. Crystal statistics. i. a two-dimensional model with an order-disorder transition. *Physical Review*, 65(3):117–149, February 1944.

[60] G. Lehaut, F. Gulminelli, and O. Lopez. Phase diagram of the charged lattice-gas model with two types of particles. *Physical Review E*, 81(5):051104.1–051104.12, May 2010.

[61] L. G. Moretto. Statistical emission of large fragments: A general theoretical approach. *Nuclear Physics A*, 247(2):211–230, March 1975.

[62] H. Pelzer and E. Wigner. *Zeitschrift Für Physik Chemie*, 35:445, 1932.

[63] E. Wigner. *Zeitschrift Für Physik Chemie*, 19:203, 1932.

[64] E. Wigner. The transition state method. *Transactions of the Faraday Society*, 31(1):29–41, January 1938.

[65] J. B. Elliott, L. G. Moretto, L. Phair, G. J. Wozniak, L. Beaulieu, H. Breuer, R. G. Korteling, K. Kwiatkowski, T. Lefort, L. Pienkowski, A. Ruangma, V. E. Viola, and S. J. Yennello. Liquid to vapor phase transition in excited nuclei. *Physical Review Letters*, 88(4):042701.1–042701.2, January 2002.

[66] J. B. Elliott, L. G. Moretto, L. Phair, G. J. Wozniak, S. Albergo, F. Bieser, F. P. Brady, Z. Caccia, D. A. Cebra, A. D. Chacon, J. L. Chance, Y. Choi, S. Costa, M. L. Gilkes, J. A. Hauger, A. S. Hirsch, E. L. Hjort, A. Insolia, M. Justice, D. Keane, J. C. Kintner, V. Lindenstruth, M. A. Lisa, H. S. Matis, M. McMahan, C. McParland, W. F. J. Müller, D. L. Olson, M. D. Partlan, N. T. Porile, R. Potenza, G. Rai, J. Rasmussen, H. G. Ritter, J. Romanski, J. L. Romero, G. V. Russo, H. Sann, R. P. Scharenberg, A. Scott, Y. Shao, B. K. Srivastava, T. J. M. Symons, M. Tincknell, C. Tuvé, S. Wang, P. Warren, H. H. Wieman, T. Wienold, and K. Wolf. Constructing the phase diagram of finite neutral nuclear matter. *Physical Review C*, 67(2):024609.1–024609.14, February 2003.

[67] K. Hagel, D. Fabris, P. Gonthier, H. Hoc, Y. Lou, Z. Majk, G. Mouchaty, M. N. Namboodiri, J. B. Natowitz, G. Nebbia, R. P. Schmitt, G. Viestie, R. Wada, and B. Wilkins. Production and characterization of hot nuclei in the reactions of 19 and 35 mev/u ^{14}n with ^{145}sm. *Nuclear Physics A*, 486(2):429–455, September 1988.

[68] Al. H. Raduta and Ad. R. Raduta. Simulation of statistical ensembles suitable for the description of nuclear multifragmentation. *Physical Review C*, 55(3):1344–3152, March 1997.

[69] Y. G. Ma, J. B. Natowitz, R. Wada, K. Hagel, J. Wang, T. Keutgen, Z. Majka, M. Murray, L. Qin, P. Smith, R. Alfaro, J. Cibor, M. Cinausero, Y. El Masri, D. Fabris, E. Fioretto, A. Keksis, M. Lunardon, A. Makeev, N. Marie, E. Martin, A. Martinez-Davalos, A. Menchaca-Rocha, G. Nebbia, G. Prete, V. Rizzi, A. Ruangma, D. V. Shetty, G. Souliotis, P. Staszel, M. Veselsky, G. Viesti, E. M. Winchester, and S. J. Yennello. Critical behavior in light nuclear systems: Experimental aspects. *Physical Review C*, 71(5):054606.1–054606.23, May 2005.

[70] T. S. Fan, K. X. Jing, L. Phair, K. Tso, M. McMahan, K. Hanold, G. J. Wozniak, and L. G. Moretto. Excitation functions and mass asymmetric fission barriers for compound nuclei 70,76se. *Nuclear Physics A*, 679(2):121–146, June 2000.

[71] M. L. Gilkes, S. Albergo, F. Bieser, F. P. Brady, Z. Caccia, D. A. Cebra, A. D. Chacon, J. L. Chance, Y. Choi, S. Costa, J. B. Elliott, J. A. Hauger, A. S. Hirsch, E. L. Hjort, A. Insolia, M. Justice, D. Keane, J. C. Kintner, V. Lindenstruth, M. A. Lisa, U. Lynen, H. S. Matis, M. McMahan, C. McParland, W. F. J. Müller, D. L. Olson, M. D. Partlan, N. T. Porile, R. Potenza, G. Rai, J. Rasmussen, H. G. Ritter, J. Romanski, J. L. Romero, G. V. Russo, H. Sann, R. Scharenberg, A. Scott, Y. Shao, B. K. Srivastava, T. J. M. Symons, M. Tincknell, C. Tuvé, S. Wang, P. Warren, H. H. Weiman, and K. Wolf. Determination of critical exponents from

the multifragmentation of gold nuclei. *Physical Review Letters*, 73(12):1590–1593, September 1994.

[72] K. Kwiatkowski, D. S. Bracken, K. B. Morley, J. Brzychczyk, E. Renshaw Foxford, K. Komisarcik, V. E. Viola, N. R. Yoder, J. Dorsett, J. Poehlman, N. Madden, and J. Ottarson. The indiana silicon sphere 4π charged-particle detector array. *Nuclear Instruments and Methods in Physics Research Section A: Accelerators, Spectrometers, Detectors and Associated Equipment*, 360(3):571–583, June 1995.

[73] J. A. Hauger, S. Albergo, F. Bieser, F. P. Brady, Z. Caccia, D. A. Cebra, A. D. Chacon, J. L. Chance, Y. Choi, S. Costa, S. Albergo, A. Insolia, J. B. Elliott, M. L. Gilkes, A. S. Hirsch, E. L. Hjort, A. Insolia, M. Justice, D. Keane, J. C. Kintner, V. Lindenstruth, M. A. Lisa, U. Lynen, H. S. Matis, M. McMahan, C. McParland, W. F. J. Müller, D. L. Olson, M. D. Partlan, N. T. Porile, R. Potenza, G. Rai, J. Rasmussen, H. G. Ritter, J. Romanski, J. L. Romero, G. V. Russo, H. Sann, R. Scharenberg, A. Scott, Y. Shao, B. K. Srivastava, T. J. M. Symons, M. Tincknell, S. Wang C. Tuvé, P. Warren, H. H. Wieman, T. Wienold, and K. Wolf. Dynamics of the multifragmentation of 1a gev gold on carbon. *Physical Review Letters*, 77(2):235–238, July 1996.

[74] T. Lefort, K. Kwiatkowski, W. c. Hsi, L. Pienkowski, L. Beaulieu, B. Back, H. Breuer, S. Gushue, R. G. Korteling, R. Laforest, E. Martin, E. Ramakrishnan, L. P. Remsberg, D. Rowland, A. Ruangma, V. E. Viola, E. Winchester, and S. J. Yennello. Heating ^{197}au nuclei with 8gev/c antiproton and $\pi-$ beams. *Physical Review Letters*, 83(20):4033–4036, November 1999.

[75] J. A. Hauger, S. Albergo, F. Bieser, F. P. Brady, Z. Caccia, D. A. Cebra, A. D. Chacon, J. L. Chance, Y. Choi, S. Costa, S. Albergo, A. Insolia, J. B. Elliott, M. L. Gilkes, A. S. Hirsch, E. L. Hjort, A. Insolia, M. Justice, D. Keane, J. C. Kintner, V. Lindenstruth, M. A. Lisa, U. Lynen, H. S. Matis, M. McMahan, C. McParland, W. F. J. Müller, D. L. Olson, M. D. Partlan, N. T. Porile, R. Potenza, G. Rai, J. Rasmussen, H. G. Ritter, J. Romanski, J. L. Romero, G. V. Russo, H. Sann, R. Scharenberg, A. Scott, Y. Shao, B. K. Srivastava, T. J. M. Symons, M. Tincknell, S. Wang C. Tuvé, P. Warren, H. H. Wieman, T. Wienold, and K. Wolf. Two-stage multifragmentation of 1a gev kr, la, and au. *Physical Review C*, 62(024616):024616.1–024616.14, July 2000.

[76] L. Beaulieu, T. Lefort, K. Kwiatkowski, R. T. de Souza, W. c. Hsi, L. Pienkowski, B. Back, D. S. Bracken, H. Breuer, E. Cornell, F. Gimeno-Nogues, D. S. Ginger, S. Gushue, R. G. Korteling, R. Laforest, E. Martin, K. B. Morley, E. Ramakrishnan, L. P. Remsberg, D. Rowland, A. Ruangma, V. E. Viola, G. Wang, E. Winchester, and S. J. Yennello. Signals for a transition from surface to bulk emission in thermal multifragmentation. *Physical Review Letters*, 84(26):5971–5974, June 2000.

[77] J. B. Elliott, L. G. Moretto, L. Phair, G. J. Wozniak, S. Albergo, F. Bieser, Z. Caccia F. P. Brady and, D. A. Cebra, A. D. Chacon, J. L. Chance, Y. Choi, S. Costa, M. L. Gilkes, J. A. Hauger, A. S. Hirsch, E. L. Hjort, A. Insolia,

M. Justice, D. Keane, V. Lindenstruth J. C. Kintner and, M. A. Lisa, H. S. Matis, M. McMahan, C. McParland, W. F. J. Müller, D. L. Olson, M. D. Partlan, R. Potenza N. T. Porile and, G. Rai, J. Rasmussen, H. G. Ritter, J. Romanski, J. L. Romero, G. V. Russo, H. Sann, R. P. Scharenberg, A. Scott, Y. Shao, B. K. Srivastava, T. J. M. Symons, M. Tincknell, C. Tuvé, S. Wang, P. G. Warren, H. H. Wieman, T. Wienold, and K. Wolf. Nuclear multifragmentation, percolation, and the fisher droplet model: Common features of reducibility and thermal scaling. *Physical Review Letters*, 85(6):1194–1197, August 2000.

[78] J. B. Elliott, S. Albergo, F. Bieser, F. P. Brady, Z. Caccia, D. A. Cebra, A. D. Chacon, J. L. Chance, Y. Choi, S. Costa, M. L. Gilkes, J. A. Hauger, A. S. Hirsch, E. L. Hjort, A. Insolia, M. Justice, D. Keane, J. C. Kintner, V. Lindenstruth, M. A. Lisa, H. S. Matis, M. McMahan, C. McParland, W. F. J. Müller, D. L. Olson, M. D. Partlan, N. T. Porile, R. Potenza, G. Rai, J. Rasmussen, H. G. Ritter, J. Romanski, J. L. Romero, G. V. Russo, H. Sann, R. P. Scharenberg, A. Scott, Y. Shao, B. K. Srivastava, T. J. M. Symons, M. Tincknell, C. Tuvè, S. Wang, P. G. Warren, H. H. Wieman, T. Wienold, and K. Wolf. Statistical signatures of critical behavior in small systems. *Physical Review C*, 62(6):064603.1–064603.33, October 2000.

[79] L. Beaulieu, T. Lefort, K. Kwiatkowski, R. T. de Souza, W. c. Hsi, L. Pienkowski, B. Back, D. S. Bracken, H. Breuer, E. Cornell, F. Gimeno-Nogues, D. S. Ginger, S. Gushue, R. G. Korteling, R. Laforest, E. Martin, K. B. Morley, E. Ramakrishnan, L. P. Remsberg, D. Rowland, A. Ruangma, V. E. Viola, G. Wang, E. Winchester, and S. J. Yennello. Signals for a transition from surface to bulk emission in thermal multifragmentation. *Physical Review Letters*, 84(26):5971–5974, June 2001.

[80] A. S. Hirsch, A. Bujak, J. E. Finn, L. J. Gutay, R. W. Minich, N. T. Porile, R. P. Scharenberg, B. C. Stringfellow, and F. Turkot. Experimental results from high energy proton-nucleus interactions, critical phenomena, and the thermal liquid drop model of fragment production. *Physical Review C*, 29(2):508–525, February 1984.

[81] J. B. Elliott, L. G. Moretto, L. Phair, and P. T. Lake. Experimentally determining the liquid-vapor coexistence curve of bulk nuclear matter (in progress). *Physical Review C*, 2011.

[82] B. Friedman and V. R. Pandharipande. Hot and cold, nuclear and neutron matter. *Nuclear Physics A*, 361(2):502–520, May 1981.

[83] N. K. Glendenning, L. P. Csernai, and J. I. Kapusta. Liquid-gas phase separation in nuclear collisions. *Physical Review C*, 33(4):1299–1302, April 1986.

[84] H. Müller and B. D. Serot. Phase transitions in warm, asymmetric nuclear matter. *Physical Review C*, 52(4):2072–2091, October 1995.

[85] M. Jin, M. Urban, and P. Schuck. Bec-bcs crossover and the liquid-gas phase transition in hot and dense nuclear matter. *Physical Review C*, 82(2):024911.1–024911.10, August 2010.

[86] C. S. Kiang. Use of liquid-droplet model in calculations of the critical exponent δ. *Physical Review Letters*, 24(2):47–50, January 1970.

[87] J. B. Elliott, L. G. Moretto, L. Phair, and P. T. Lake. The unreasonable accuracy of fisher's droplet model (in progress). *Journal of Chemical Physics*, 2011.